Politecnico di Torino

Master's Degree in Energy And Nuclear Engineering

CFD validation of a new gas turbine stage design with experimental data

Master's Degree Thesis

Supervisors

Prof. Mirko Baratta

Dr. Jens Fridh

Candidates

Claudia Florentina Balan

23 March 2022

*Even when it is hard, remember that studying
it's a privilege that not everybody has.*

Abstract

Gas turbines are present in two energy-intensive sectors: aviation and energy production. Improving the efficiency of gas turbines has a huge impact on the reduction of CO2 in the atmosphere, therefore many research groups are studying innovative strategies to improve the performance of these turbines. This thesis work concerns the evaluation of the global performance of a test turbine located in the laboratory of the Unit of Heat and Power Technology of the Royal Institute of Technology (KTH), commissioned by Siemens Energy. The innovative features of this turbine are the presence in the rotor of a more three-dimensional geometry of the blades, of a non-axisymmetric endwall contouring for the reduction of secondary losses and a reduced blade count compared to previous stage for the same power requirements. The performance evaluation is done both with experimental tests and using CFD simulations. The current efficiency is compared with that of the previous rotor blisk to understand if there has been an improvement or deterioration in performance. Furthermore, a comparison was also made between the results of the experimental tests and simulations, justifying possible discrepancies.

Acknowledgements

Table of Contents

List of Figures

List of Tables

Acronyms

CAD	Computer aided Design
CCHT	Combined cycle gas turbine
CFD	Computational fluid dynamics
CHP	Combined heat and power plant
DNS	Direct numerical simulation
ISO	International Organization for Standardization
KTH	Kungliga Tekniska högskolan (engl. Royal Institute of Technology)
LES	Large Eddy Simulation
MF	Mass flow
PT100	Platinum resistor thermometer with 100Ω at $0°C$
RANS	Reynolds averaged Navier-Stokes
RNG	Re-Normalisation group methods
RPM	Revolutions per minute
SST	Shear Stress Transport turbulence model
TS	Total-to-static
URANS	Unsteady RANS

Chapter 1

Introduction to gas turbines

Gas turbines are a fundamental part of everyday life in modern society. They are one of the fundamental components in power generation and aviation sector. A gas turbine can be defined as a device powered by a liquid or gaseous fuel in order to produce combustion energy, which can be transformed into electricity by a rotating shaft and a generator, or alternatively, into mechanical power for ship propulsion or for driving compressors in an aircraft jet engine [1].

Starting from the **aviation sector**, most of the aircraft engines are currently gas turbines as, for example, in civil and military aircraft, helicopters and business jets [2, 3, 4]. The wide diffusion is due to the great reliability of the gas turbines, also accompanied by a good weight ratios. Therefore, reciprocating engines remained limited to small aircraft only [5].

Moreover, in recent years, gas turbines have also played an increasingly important role in the **production of electricity** from fossil fuel sources [6, 7, 8], since traditional steam plants have been gradually replaced by more efficient combined heat and power plants (CHP). In addition to these two main applications, gas turbines are present in other minor applications such as power pumps and compressors for the transport of oil and gas or for rather fast military ships, thanks to their good power/weight ratio which makes them more suitable for this purpose [9].

Taking part in two very **energy-intensive** sectors, gas turbines are involved in the creation of large quantities of CO_2 emissions, around 50% of the total emissions in the world: 41% coming from the production of electricity and about 3% due to aviation sector [10, 11, 12]. If the new, more ambitious limits on emissions are to be respected in the near future, it is important to develop better performing and more efficient gas turbines. To comprehend the huge impact of improving a **plant's efficiency**, a 1% increase in efficiency for a plant with gas fired combined-cycle gas turbine (CCHT) of 1000 MW, leads to a reduction of 50 000 tons CO_2/year! It is therefore easy to understand the motivation that drives many research groups to pursue an **improvement of the performance** for the new gas turbines [13].

1.1 Energy generation

In the power generation sector, gas turbines are present in a wide variety of capacities and configurations, ranging from microturbines to large turbines for power generation in power plants. In particular they are suitable for CHP applications because the hot exhausted gases can be used to generate high pressure steam for industrial heating or drying processes, or for heating residential buildings through a similar system as the one depicted in *Figure 1.1* [14].

Alternatively, the heat recovered through the **steam generation** systems, can be converted in electricity. In this case, the gas turbine is the first component that comes into contact with the combustion products that are at high temperatures. Together with the generator it converts the combustion energy into electricity, corresponding to two thirds of the total output power produced by the plant. The remaining heat in the **hot exhaust gas** is used to feed a boiler that makes steam for a secondary circuit and a steam turbine used to produce the remaining one third of the plant's power output. While increasing the complexity of the plant, also the efficiency grows, balancing the increase in the cost of the plant [15].
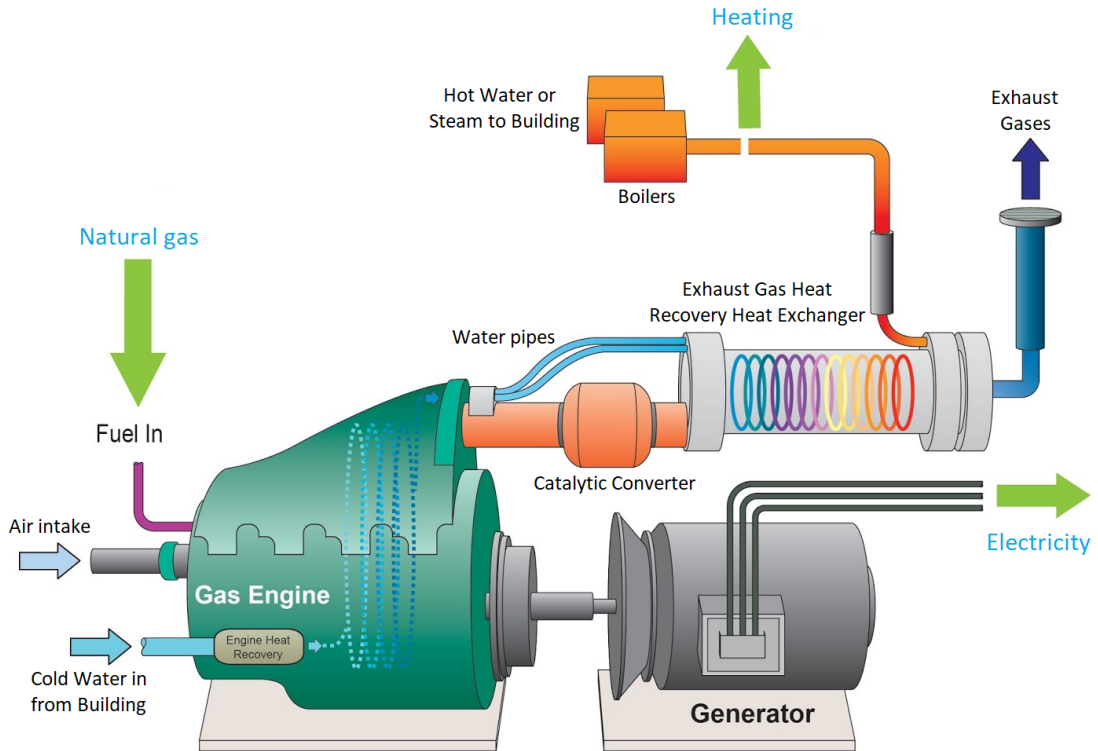
Figure 1.1: Cogeneration power system (in courtesy of Simons Green Energy)

1.2 Worldwide reduction of CO_2 emissions

Gas turbines are establishing themselves as the best alternative to produce electricity from fossil fuels, not only because of their great involvement in the most energy-intensive sectors of society, but also because they have some better characteristics compare to the ones of traditional coal-fired power plants. There is great potential in reducing CO_2 emissions in the next years by implementing retrofit policies, replacing old coal-fired plants with new, efficient gas turbine plants.

1.2.1 Natural gas

In addition to their increasing efficiency, gas turbines are the favorite technology among those for the conversion of energy from **fossil sources**, for employing a more sustainable type of fuel: natural gas. At the moment gas is the second fossil source from which electricity is produced after coal, that had dominated the power production in past years. In already economically developed countries, a conversion of coal-fired power plants into gas-fired power plants is taking place.

The first reason for this trend is the **price**: for example, in the United States, new gas deposits have been increasingly exploited and that have increased the availability of natural gas, reducing its cost. The second reason is connected to **carbon dioxide** emissions: the use of natural gas leads to the production of significantly less CO_2 than coal. Investing in new gas plants, replacing coal-fired ones, has allowed many companies to meet climate-change emission control limits.

The next step for the power generation from low emissions systems is to add carbon capture and storage technologies to gas-fired power plants [16, 17, 18].

1.2.2 Energy transition

Another indirect way to reduce CO2 emissions by using gas turbines, is to have a good **backup system** for renewable resources in order to guarantee the correct operation of the electric grid. A greater share of solar and wind in the electricity generation is not possible without a fast-reacting backup system to compensate the intermittent nature of these resources and stabilize the grid [13, 16].

However, this new way of using gas turbines implies a change in the operating time of gas turbines: from 12 starts per year and 8000h of operation in the past, now the power varies continuously with the load curve which results in more than 250 starts per year and about 3000h of operation. Working mainly at **partial load**, the turbine has lower efficiency, higher cost, fatigue deterioration and increased CO_2 and NO_x emissions. For this reason, the research is already focusing on improving the performance of gas turbines in partial load operation [19, 20, 21].

1.3 Future trends

In recent years, the performance of gas turbines has been ameliorated due to substantial investments in research and development, in terms of conversion efficiency, plant capacity, availability and reliability [22]. These achievements have been possible by improving the **performance and aerodynamics** of the blades.

One of the most effective methods to have a more efficient turbine is to increase the inlet temperature of hot gases, possible thanks to the introduction of new materials, coatings and cooling technologies. Besides, another major development driver has been the evolution of manufacturing technologies that allowed the creation of more complex and aerodynamic geometries [23, 24, 25]. The design of modern turbines employs **advanced strategies** in line with current trends and they present some recurring features that are listed below:

1. Non-axisymmetric endwall contouring.

2. Reduced number of blades.

3. Advanced tip clearance reduction.

4. Complex cooling strategies.

5. Advanced materials, coatings and manufacturing technology.
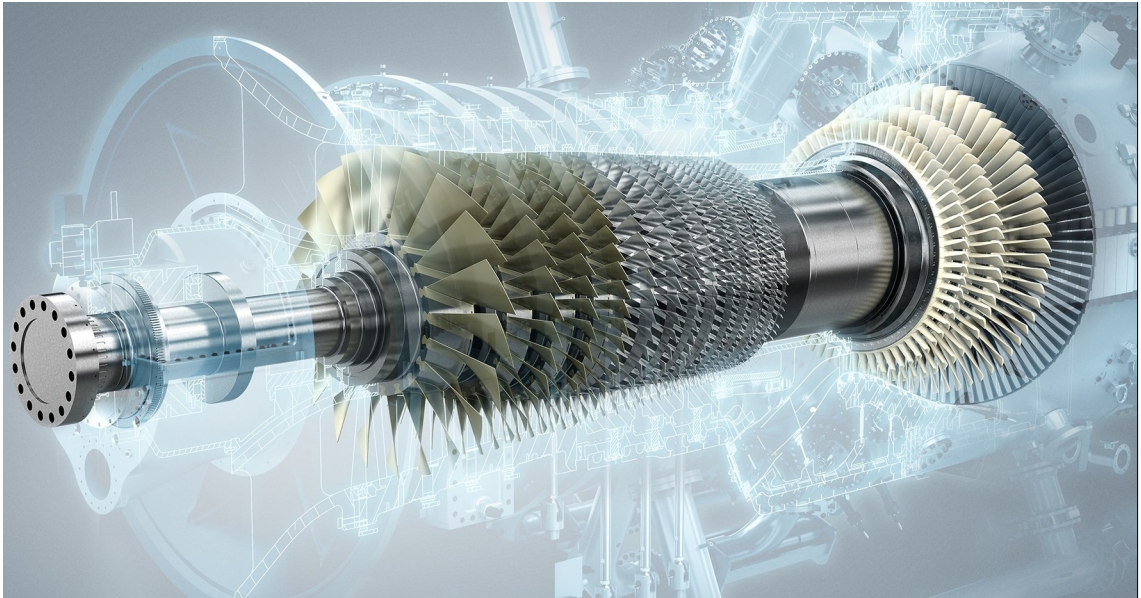
Figure 1.2: Advance turbine blade profiles (in courtesy of Siemens Energy)

Chapter 2

Research outline

2.1 Research gap

As mentioned, there are many paths to further develop advanced turbines with very high efficiency. One of the strategies suggested is, for example, building complex **three-dimensional geometries** with **non-axisymmetric** endwall contouring. There is not yet a geometry perfectly optimized for every possible operating condition. For this reason, the performance of new turbines has to be verified first with tests on prototypes before commissioning the full size turbines.

2.2 Research objectives

The research of this report is part of the aforementioned industrial context, having as its objective to **evaluate the performance** of a new blisk rotor for a gas turbine. For this purpose, experimental tests will be carried out, accompanied by CFD simulations. The experimental trials will give a realistic representation of the operation of the system, while obtaining a validated CFD model is important in order to have a detailed description of the fluid flow. Using this model it is possible, for example, to study the causes for the formation of aerodynamic losses or in future as starting point for the design of a new turbine geometry. In order to achieve this result the process can be divided in these sub-objectives:

- Mesh generation for the new blisk and CFD simulation of the flow.
- Experimental trials with the same operating conditions as CFD simulations.
- Elaboration of results through performance indicators.
- Validation of the CFD model with experimental results.
- Comparison with the performance of the previous blisk.

2.3 Research hypothesis

The expected result is to have an **improvement** in the performance of the turbine compare to the previous one, thanks to the advanced strategies used such as non-axisymmetric endwall contouring and a reduction in the number of blades. These characteristics are known from the literature to bring a decrease of the aerodynamic losses and an improvement of the performance.

In addition, the results from experiments and CFD simulation are expected to be **similar**, if the meshing and simulation techniques are enough accurate.

2.4 Research methodology

At the moment the test turbine is part of a research project in a collaboration between KTH and Siemens Energy. Specifically, the component analyzed is the **rotor disc** of a new gas turbine, inserted in the test facility in operation in the Department of Energy Technology of the Royal Institute of Technology KTH since 1989 [26]. In particular, the **test facility** will be used to obtain the experimental results of the analysis.

As for the simulations, it was decided to reduce the domain by exploiting the periodicity of the domain, extracting a section, corresponding to a single blade. This will allow to obtain a more accurate solution, with the same computational time by increasing the mesh refinement. The mesh is generated with the software Autogrid5 [27]. This will be the starting point for the actual **simulation** of the system which will be processed in Ansys-CFX [28], commercial CFD software.

The performance will be evaluated in terms of efficiency and degree of reaction of the system for different values of the isentropic velocity and flow coefficient. It will be important to have the same input conditions and the same definition of performance for experimental tests and simulations so as not to generate discrepancies between the results due to a method error. The **comparison** will be in the end also made between the experimental method and the simulations and between the current blisk (object No.6) and the previous one (object No.5).

2.5 Scope and limitations

There are many aspects that can be taken into account when analyzing a turbine: the thermodynamic, aerodynamic, mechanical performance, materials, economic benefits (aiming for example at the maximum production of work, with the use of the minimum possible flow for cooling). A complete study is too long for a thesis report, for this reason it was decided to limit the study to **aerodynamic** performance and characteristics.

Chapter 3

Theory: axial turbines

The turbine performance has often been mentioned in previous chapters, but to better understand how to evaluate the overall performance of the system, it is necessary to take a step back for a more detailed description of gas turbines. Understanding the parameters that affect the efficiency will serve to better understand the strategies that lead to an improvement or loss in performance and to find the direction for further development of the technology.

3.1   Operation

Axial turbines are a set of one or more stages, each consisting of a stator and a rotor equipped respectively with nozzle guide vanes and rotor blades. The surface area of the rotor passage, at a smaller radius, is called *hub*, while the upper limit of the main annulus for the flow is the *shroud*.

The high enthalpy of the incoming fluid is converted into useful shaft torque thanks to the expansion and motion of the fluid inside the turbine blades, which results in a rotary motion of the rotor and its shaft. In most cases the **stator** vane purpose is to accelerate the flow. This is done by changing the direction of the flow from axial to tangential, thereby changing the flow area and increasing the potential extracted work. By the laws of conservation of mass, this profile leads to an increase in velocity. The **rotor** is designed instead to maximize the creation of torque in the shaft connected to the rotor, turning with the same angular speed. The rotor is characterized by a tangential speed, as can be seen in the *Figure 3.1* from [29], that is strongly related to the useful effect of the turbine.

To evaluate the performance of the turbine often not only the pressures values are used, but also the fluid **velocity**, especially in the process of aerodynamic design of the shape of the blades. In the next paragraphs the components of velocity and the correlations to calculate their specific work will be further specified.

3.2 Velocity triangles

Figure 3.1 shows the profile of the blades for the stator and rotor in a cross section of the blade at **constant radius**, giving a two-dimensional view of the aerodynamic profile of the blade. It should be noted that modern turbines have a strongly three-dimensional profile, therefore the profile changes considerably in the different cross sections. Unless noted othrerwise, it is usually taken at mid-span.
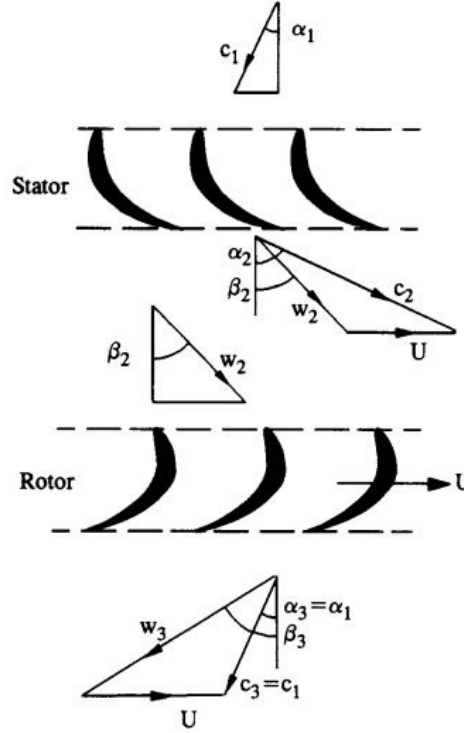
Figure 3.1: Velocity triangles for stage

The velocity triangle represents the **velocity components** of flux in an absolute and relative system. Absolute velocities are denoted by the letter c and have inclination α relative to the axial (vertical) direction. In addition, for the rotor a relative system can be used that rotates with tangential velocity u. The relative velocity component is called w and is tilted relative to the axis of an angle β. The stator is fixed therefore there are only absolute speed components, while for the rotor the absolute speed is decomposed into the vector sum of the relative component and the rotation speed. The velocity triangle is an important tool in **blade design**. The angle by which the stator blade is inclined is equal to that of the absolute velocity. While for the rotor the angle of which the blade is inclined is equal to the relative velocity of the flow at nominal conditions.

3.3 Specific work

The useful effect, that can be extracted from the passage of a hot air flow between the blades of a gas turbine, is to **produce electricity**. This form of energy is actually the result of some intermediate transformations: the thermal and kinetic energy of the fluid is converted into a rotary movement of the rotor and this mechanical work is transmitted by a shaft connected to the rotor and generator and transformed into electrical energy.

In particular, the **work** extracted from the fluid is generally proportional to the change in tangential velocity in the rotor. This can be proved in the first place by following the **Newton second law of motion**, which states that the rate of change in momentum of a mass is equal to the sum of the forces acting on it:

$$\sum \overrightarrow{F} = \frac{d}{dt}(m\overrightarrow{c}) \tag{3.1}$$

Both the rotor and the stator are subjected to a reaction force, since in both there is a change in velocity. However, the stator is constrained, preventing its rotation, therefore it is not able to rotate, while the rotor is mounted on a shaft that allows to take advantage of the rotational movement that is established. The power output is calculated by applying Eq.3.1 in the direction in the tangential direction, obtaining the Eq. 3.2:

$$\tau = \dot{m}(r_3 c_{3\theta} - r_2 c_{2\theta}) \tag{3.2}$$

Since, as mentioned earlier, the triangle of velocities is given for a section at a given radial location, both the torque τ and the tangential speed u depend on the radius. By identifying u as the product between angular velocity and radius, the above equation can be rewritten as Eq. 3.3:

$$\tau\Omega = \dot{m}(u_3 c_{3\theta} - u_2 c_{2\theta}) \tag{3.3}$$

The product of angular velocity and torque is the shaft power, which can be related to the specific work extracted through the rotor, dividing both members of the Eq. 3.3 for the mass flow rate. The work has a positive sign when the enthalpy of the fluid entering the rotor is greater than the outgoing one, resulting in the next formula (Eq. 3.4), named **Euler's turbine equation**:

$$W = u_3 c_{3\theta} - u_2 c_{2\theta} = h_{01} - h_{03} \tag{3.4}$$

Assuming adiabatic conditions and isentropic expansion, the enthalpy of the flow is entirely used in order to extract work from the flow.

3.3.1   Non-isentropic expansion

In a real case it is necessary to consider both thermal and aerodynamic losses that will decrease the power output. The first effect from the presence of losses is a reduction of the entalphy difference that is effectively transformed into work. Another way to see the same problem is that losses lead to a reduction in the tangential velocity. Both these phenomena justify a reduction in turbine performance, applying the Euler equation (Eq. 3.4).

Entalpy: The difference in enthalpy in the ideal (isentropic) and real (non-isentropic) case is analyzed in more detail. In *Figure 3.2 b* [29] losses are named $\Delta h_{o,l_{oss}}$ and the difference of enthalpy transformed into work (Δh_o) is defined as the product between the available entalphy of the stage ($h_{01} - h_{03s}$) and a reduction factor η_{is}, which is called isentropic efficiency according to the following equation:

$$W = \eta_{is}(h_{01} - h_{03s}) \tag{3.5}$$

The isentropic efficiency can vary between 0 and 1, being 1 the ideal case in which the process is isentropic. This term includes only aerodynamic and thermal losses, while the mechanical or electrical losses are neglected at this point. The origin of aerodynamic losses will be explained in the next paragraph, along with some strategies from the literature in order to reduce them.
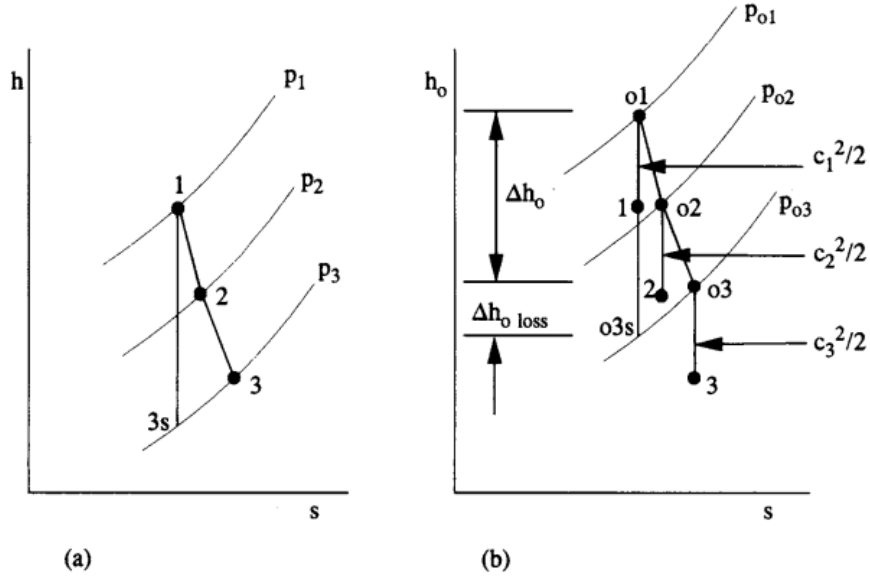
Figure 3.2: Enthalpy drop for a real case: (a) static (b) total

10

3.4 Aerodynamic losses

Over the years enormous efforts have been made to maximize the efficiency of all types of turbomachines, obtaining for large machines a total-to-total efficiency above 90%. Further improvements can always be made thanks to the deeper understanding of fluid dynamics and thermodynamics of the flow, even if they are increasingly difficult to obtain. The thermodynamic explanation of the reason why a real process differs from the ideal can be connected to the **generation of entropy**, which can be seen as wasted energy. A great contribution in the analysis of entropy generation in turbomachinery have come from Denton [30] who studied in detail the process of losses formation.

3.4.1 Mechanisms for entropy generation

Entropy formation occurs whenever a process presents viscous forces, acceleration/deceleration or situations of thermal non-equilibrium. Specifically, there are three main causes for the entropy generation:

- Viscous friction in boundary layers or free shear layers, which can for example be a mixing process or a leakage jet.

- Heat transfer between two sources that have a finite difference in temperature, such as when mainstream flow mixes with coolant gas.

- Non equilibrium processes such as a rapid expansion or shock waves.

In turbines, viscous effects and non-equilibrium processes play a fundamental role in the generation of entropy. In addition, there are **thermal losses** between areas at different temperatures, but this happens mainly for large cavity flows (e.g. coolant flows). However in this chapter the thermal losses are not considered.

3.4.2 Profile losses

To have a more simplified description of the problem, losses are divided into three main categories: *profile loss, tip leakage loss and endwall loss.* One can talk about these losses as if they act independently even if in reality they are related.

The *profile loss* is often referred to as the entropy generated within the laminar and turbulent **boundary layer**. The magnitude depends on the velocity of the free stream, roughness, Reynolds number and area of the blade [31]. **Trailing edge** losses and shock losses are included in this category. According to the two-dimensional flow theories of Denton [32] and Zweifel [33] there is an optimal pitch to chord ratio that minimizes profile loss, varying the surface velocity distribution on the blade. This is a first strategy for reducing aerodynamic losses.

3.4.3   Tip leakage loss

One of the effects of tip leakage, for both shrouded and unshrouded blades, is a reduction of the **mass flow** passing through the blade passage. Moreover, the blade loading decrease also due to the reduced length of the blade and since the **blade loading** drops off towards the tip. Numerical calculations show that this is not only confined to the tip region but it affects all the span. The effects are most noticeable in the case of an unshroud blade [34, 35, 36].

The creation of entropy is mainly caused by mixing processes between the leakage flow and the mainstream both because there is the formation of a jet during the input (see *Figure 3.3* from [30]), or simply because the two flows have different speeds, thus creating a speed gradient that leads to entropy generation.
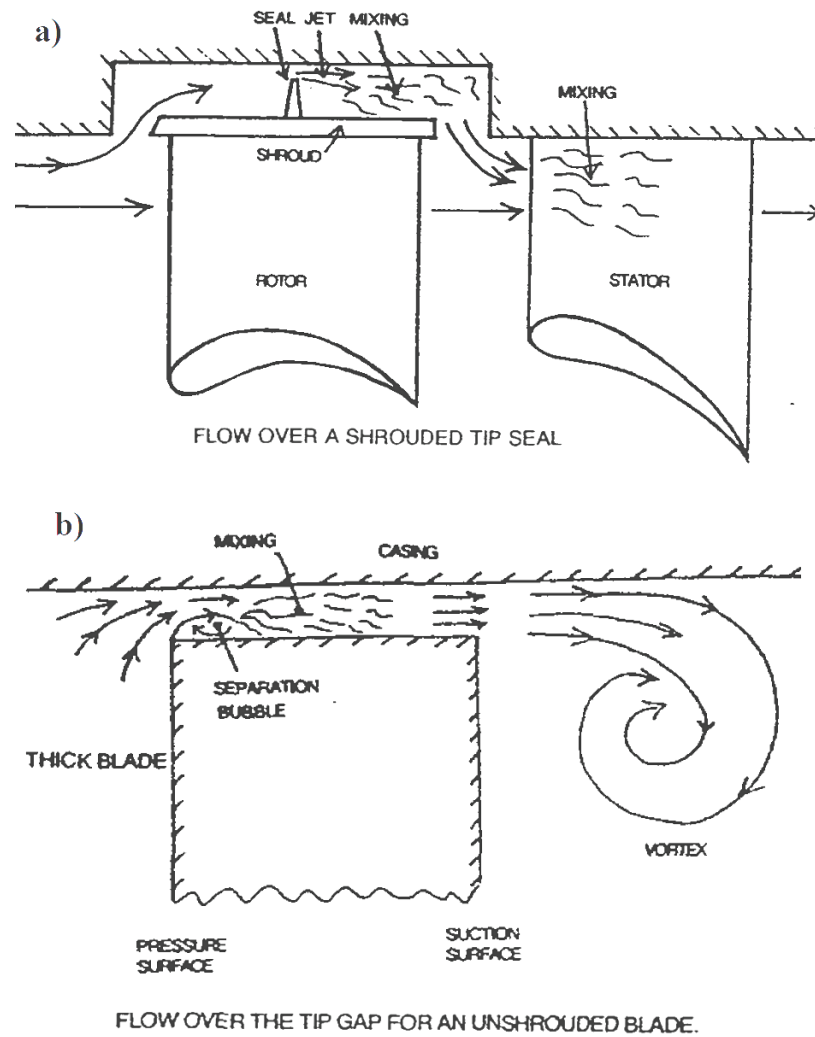
Figure 3.3: Tip leakage losses for shrouded (a) and unshrouded (b) blade

3.4.4 Endwall loss

The term "endwall loss", or "secondary loss", is used to indicate the entropy production on the annulus walls (hub and casing) due to **secondary flows**, which are the result of the endwall boundary layer entering the turbine cascade and dividing across the leading edge. Sieverding [37] and Langston [38] give an extensive review on the topic. In particular, in *Figure 3.4* from Sieverding's article, it can be seen how complex the secondary flow is, from presence of vortices with strong three-dimensionality. Especially, for stages with short blades the secondary flow is dominant in the annulus, resulting in very high endwall losses. In general, endwall loss is a great source of lost of efficiency, contributing about 1/3 of the total loss.

Recently researchers [39, 40, 41, 42] have suggested the introduction of **endwall contouring**, as a solution to limit the formation of these losses obtaining positive results. An example of endwall contouring is highlighted in *Figure 3.5* from [40].
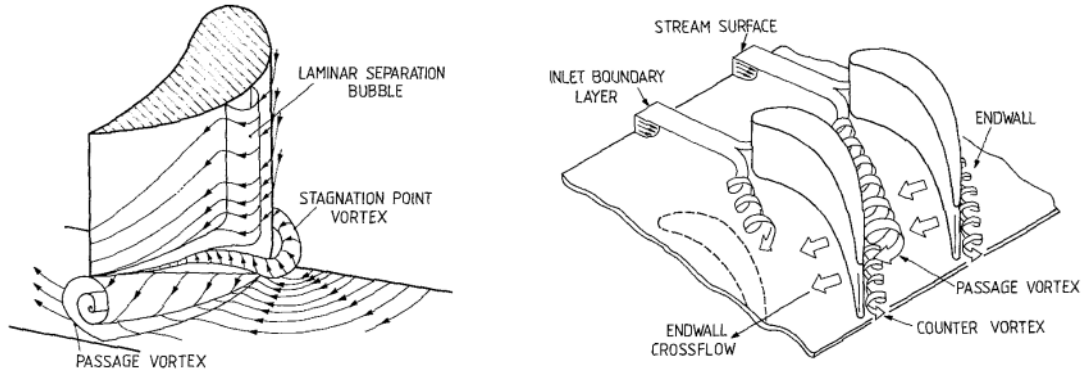
Figure 3.4: Endwall flow models by Klein and Langston
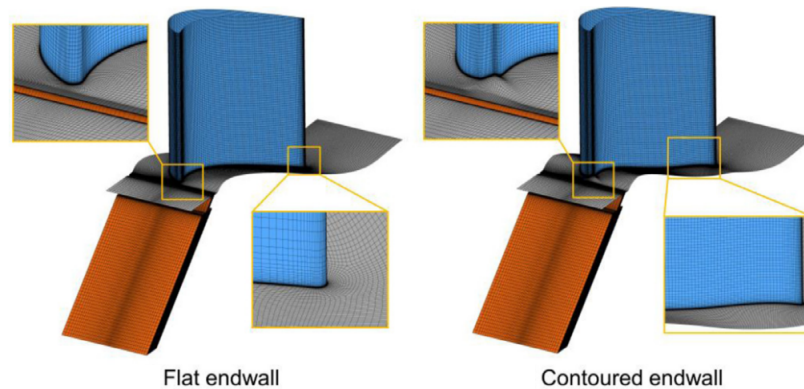
Figure 3.5: Endwall contouring: strategy for losses reduction

13

Chapter 4

CFD simulations

In the past, experimental and analytical methods have been used to solve fluid dynamic problems. In recent years, thanks to a continuous evolution of computers, computational fluid dynamics (CFD) modeling has become one of the three basic approaches used to solve fluid dynamics and heat exchange problems. Although the analytical method is still used by many and the experiments are still performed, the trend is towards a greater use of the computational approach for industrial design. This is due to the fact that CFD has peculiar characteristics that make it a fast and at the same time accurate method. In particular it is possible to:

- Approximate solution to the governing equations for complex fluid flows.
- Have a more cost-effective approach.
- Simulate conditions that are not reproducible in experimental tests.
- Provide detailed, visualized, and comprehensive information of the flow.

For all these reasons, CFD is now used in countless research and industrial fields such as: aerospace, automotive, biomedical, power and many others [43, 44]. In the early stages of the development of CFD methods, users were required to create codes for solving the problem. Later, gaining more interest from industries and researchers, commercial softwares were developed that allow the user to avoid the problems of coding, greatly accelerating the solution of fluid dynamics problems. Some of the most common commercial softwares nowadays are: Ansys CFX, Ansys Fluent, Comsol, Flow Science FLOW-3D and ESI Group CFD-ACE.

In this chapter it will be explained why it is so important to use CFD for the study of turbulent flows and what are the computational limits at the moment. To conclude, the procedure for making a CFD simulation will be briefly described, going more into details on one of the most critical steps that is the mesh generation.

4.1 Introduction to turbulence

The observation of turbulent flows is something that people experience every day and associate with non-stationary, irregular and chaotic flow of a fluid. The smoke of a cigarette in its upward motion, the mixing of milk and coffee inside a cup or the irregular wake of a river downstream of a bridge pylon are just a few examples. Although the concept of turbulence is clear, the effect that turbulence has on the global characteristics of a flow it is not equally clear [45].

By observing a turbulent flow one can immediately notice complex rotational structures which represent a peculiarity of this regime of motion and which go by the name of turbulent eddies. In particular, they appear when the flow is characterized by high Reynolds' number. Large-scale vortex structures appear on different time and space scales, interacting and exchanging energy. The largest scale contains most of the kinetic energy of the flow. As larger structures are broken down into smaller structures, this energy will gradually transfer to smaller scales.
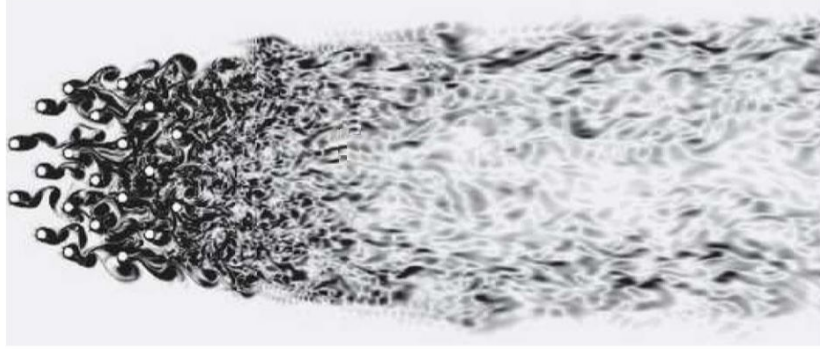
Figure 4.1: Energy cascade representation

The transfer process of energy from large scale to small scale is called direct energy cascade, and continues until viscous dissipation can convert kinetic energy into thermal energy. The scale at which this happens is called the Kolmogorov length scale [46], named after the mathematician Andrey Kolmogorov, who studied the energy cascade in turbulence (visible also in *Figure 4.1* from [47]).

Since the scale of the equation to be solved is very small, from the fine-scale dissipative motion to the complete flow, it can only be solved by the numerical approximation of the Navier-Stokes equation [48, 49].

Considering that the solution will be obtained through software that automatically implements the problem-solving method, the type of approximation method used is discussed. All theories about governing equations, geometric discretization and equations can be found in the literature [50, 51, 52, 53, 54].

4.1.1 Modeling turbulence

The governing equation of fluid flows, the Navier-Stokes equations, can be solved directly without using any modeling assumptions. This method is called Direct Numerical Simulation **(DNS)**. It needs to solve a wide range of time and space scales of turbulence, from very large to very small, up to the Kolmogorov length scale. It can be estimated that the grid resolution and time step required to correctly solve the complexity of the fluid structure are approximately proportional to the cube of the Reynolds number. This makes the DNS method infeasible to use for engineering applications, at least at the moment. DNS is indeed used almost exclusively in **academia and research** institutions to model simple flows, and together with experiments are used to understand more in deep turbulence and develop more simplified turbulence models, which have have lower computational cost and accuracy. In the rest of the report we will focus mainly on the latter [55].

In many engineering applications, it is interesting to know the mean or integral of the solution, as for example the force acting on an object or the mass flow through a channel. In order to obtain such a quantity, the use of an **average turbulence model** to solve for turbulence is recommended, as this allows a reliable solution to be obtained in a more effective and cost-effective manner. Examples of this kind of model are: RAN, RANS-LES, LES and they are sorted in *Figure 4.2* from [56] by computational time and numerical error of the results.
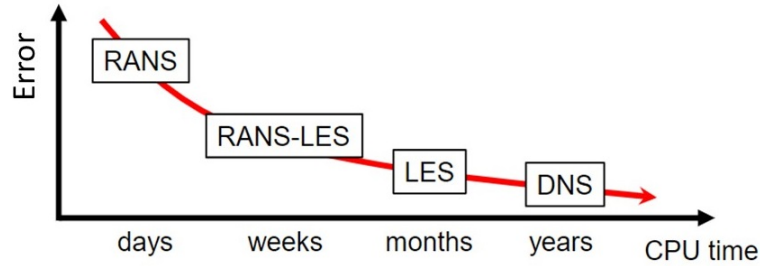
Figure 4.2: Time vs error for different approximation methods

As the number of degrees of freedom to solve the flow increases, the computational cost of CFD simulation increases from RANS to DNS. Due to the high **computational cost**, scale resolution methods such as DNS and LES are usually applied to simple geometric structures and academic configurations, while hybrid RANS-LES, URANS, and RANS can be applied to complex industrial problems. For this reason, the most used commercial software have implemented RANS based turbulent models, among which the most popular two-equation turbulence models are **k-epsilon** and **SST k-omega**. However, in future it is expected that there will be more commercial applications, of the LES methods, therefore it is relevant to evaluate their characteristics more into details.

4.1.2 Comparison RANS and LES

An averaging operation can be applied to the Navier-Stokes equation to obtain the **Reynolds Averaged Navier-Stokes** (RANS) equation. These are similar to the original equations, but include some additional terms in the momentum equation, called Reynolds stress terms, which are unknown and need to be modeled. Turbulence models are designed to express the effects of turbulence by closing the unknown Reynolds stress term. They are usually classified according to the number of additional equations required to simulate the effects of turbulence on the flow. RANS modeling is the most widespread method in industrial applications, even if the accuracy level is lower than LES and DNS, as seen in *Figure 4.3* from [57].
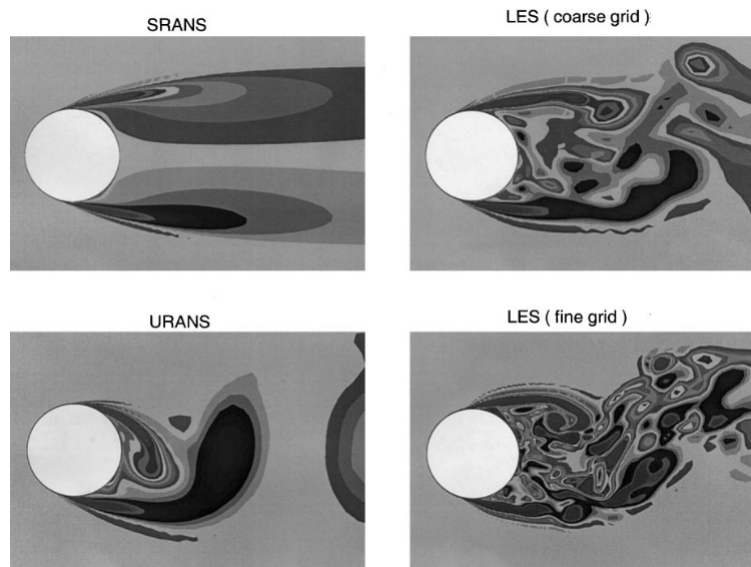
Figure 4.3: Simulation of flow past circular cylinder with RANS and LES methods

For some applications, it may be necessary to use more detailed methods, trying to resolve at least the structures that contain the most energy in the flow. This method is called **Large Eddy Simulations** (LES). The smallest scale of turbulence is filtered out in space, while the largest scale containing the most energy is directly resolved. Similar to the RANS modeling, in the LES turbulence model, the unknown term in the filtered Navier-Stokes equation is called sub-grid-scale stress, because the filter of the equation is obtained at the grid size level and will be built. The mode is degraded to a smaller flow scale than the grid size. Due to the nature of turbulence, on a very small scale, even in different applications, the flow structures are often similar to each other. LES modeling has a higher solution fidelity and applicability, but due to time step requirements, all of these are accompanied by an increase in computational cost.

4.2 CFD solution procedure

Looking at the problem from a user point of view, that has to use a CFD software, in this chapter is explain briefly the procedure for solving fluid dynamic problems with the commercial softwares currently available. According to Tu et al. [58] there are three main elements in a CFD simulation: preprocessor, solver, postprocessor as it represented in *Figure 4.4*.

The user has a fundamental role in setting the preprocessor. Starting from the **computational domain**, this is usually larger than the geometry itself to facilitate setting more stable boundary conditions. After that, the discretization of the domain is called **mesh generation** and is a very important phase because it has a great impact on the accuracy of the results and on the simulation time. A more detailed description of this phase is provided in *Chapter 4.3*. Finally, the definition of the **boundary conditions** is not a particularly complex procedure, but if performed incorrectly can lead to unrealistic results.

As for the **solver and the postprocessor**, the user must be well aware of how to read the convergency control parameters and evaluate if the results obtained are reasonable, skills that can be acquired and improved with experience.
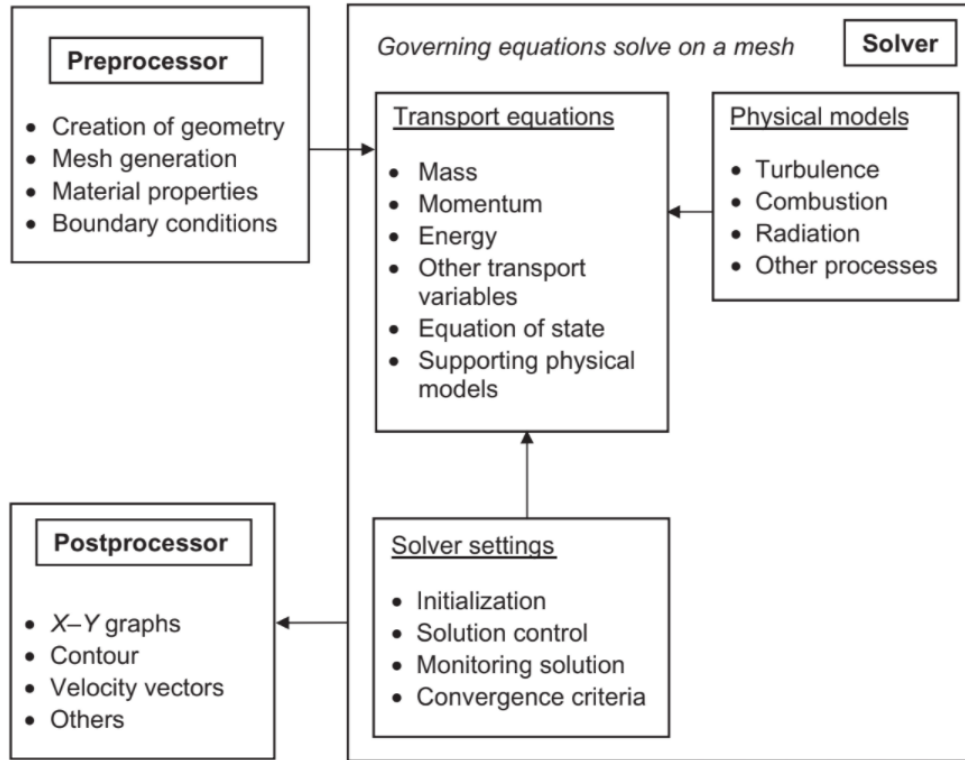
Figure 4.4: The three main parts of a CFD analysis

4.3   Mesh generation

Mesh generation represents an important step in obtaining a correct numerical solutions. It must be fine enough to capture the important **flow characteristics** and geometrical structure. In particular, for flows with bounded walls, a refinement of the mesh is suggested in the areas where there is the generation of vortices or steep flow gradients, such as near the boundary walls.

While the grid (and therefore the solution) gets more accurate by increasing the density of cells in the areas of interest (grid adaption), the main problem is that also the simulation time becomes longer. Therefore the objective is to maximize the solution **accuracy** of the solution with the lowest **number of cells**. To do this, different strategies can be used such as:

- Blocking: to specifically manage areas with flows with different characteristics.

- Wall functions: for a good refinement of the mesh at the boundary layer.

- Mesh sensitivity analysis: to find the minimum number of cells of the mesh for which the solution converges with an acceptable **quality** of the mesh.

4.3.1   Blocking

To best adapt the mesh to the flow characteristics, a possible approach is to divide the domain into areas that are managed differently. The example in *Figure 4.5* shows how blocking is set by default in the software AutoGrid5 [27]. The region surrounding the blade (skin block) has a **finer mesh** for the analysis of boundary layers and near the leading edge and trailing edge, where there are higher speed gradients. In the other areas the mesh is simpler and less refined, to save **computational time**. For more advanced users the blocking procedure can also be carried out manually, using specific softwares, as for example, ICEM.
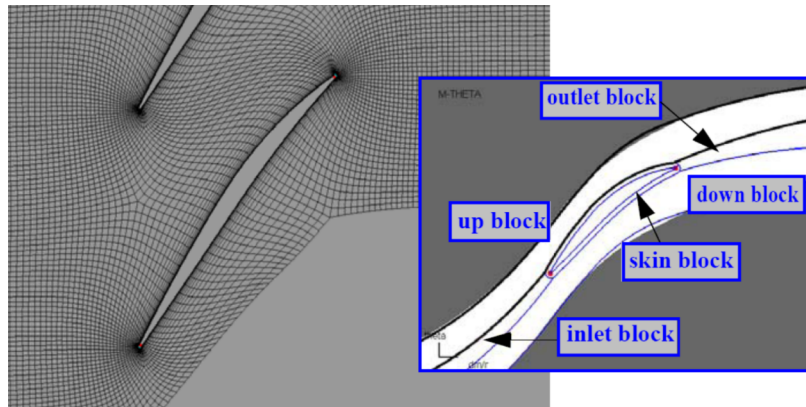
Figure 4.5: Default mesh blocking for turbine blades in Autogrid (User Manual)

4.3.2   Boundary layer: wall functions

Turbulent flows are significantly affected by the presence of walls, where the viscosity-affected regions have large velocity gradients. An accurate representation of the near wall region determines a successful prediction of wall bounded turbulent flows. In order to deal with the near wall region, two methods are proposed [59]:

1. **Turbulence models** are modified to enable the viscosity-affected region to be resolved with all the mesh down to the wall, including the viscous sublayer. The first cell center must be placed in the viscous sublayer leading to the a large number of mesh cells. Substantial computational resources are required.

   - Use low-Re model like $k - \omega$
   - Good when interested in the forces on the wall (aerodynamics analyses for F1 cars, blade optimization in turbomachinery, etc.)

2. Another way is to use **wall functions**, which are equations empirically derived and used to satisfy the physical laws near the wall. The first cell center needs to be placed in the log-law region to ensure the accuracy of the results. When using the wall functions approach, there is no need to resolve the boundary layer causing a significant reduction of the mesh size.

   - First grid cell needs to be $30 < y^+ < 300$.
   - Use high-Re model (Standard $k - \epsilon$, RNG $k - \epsilon$)
   - Use when interested in the mixing rather than the forces on the wall.
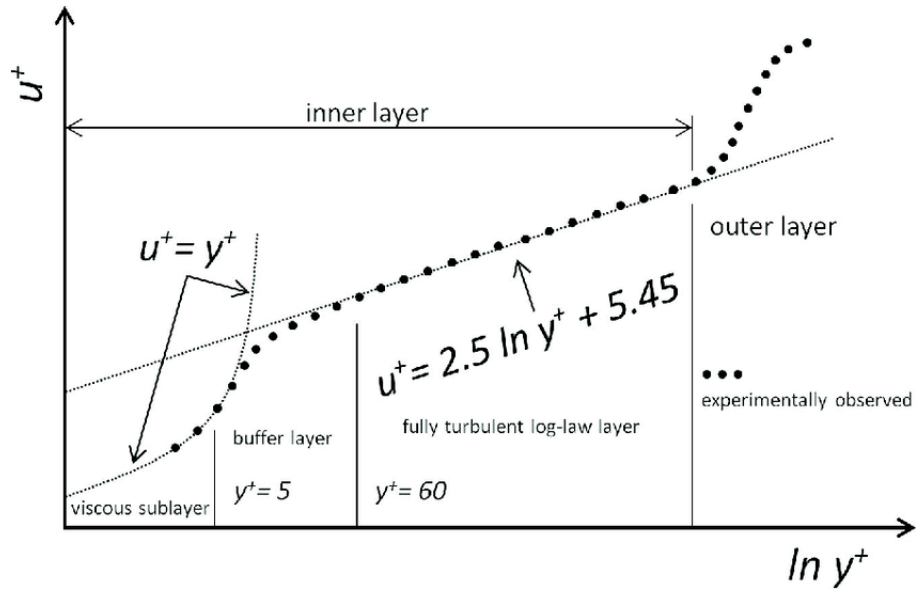
Figure 4.6: The law of the wall adapted from ANSYS User guide

4.3.3 Mesh sensitivity analysis

When performing a simulation it is important to remember that the result is the numerical solution of a problem that is posed by defining mesh and boundary conditions. The more refined the mesh, the more accurate the converged solution will be. A method to check the **convergency** for a mesh independent solution is to plot a graph of the resultant goal value vs cell count in the simulation as the one in *Figure 4.7* [60]. Good results are obtained for $N > 10^6$ Elements.
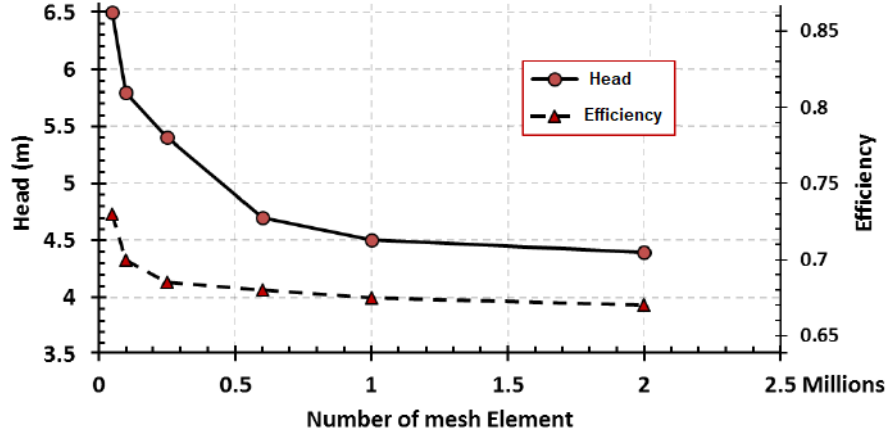
Figure 4.7: Example of convergency of the mesh

The objective of the mesh sensitivity analysis is to have an accurate solution and with the **fewest number** of cells possible, therefore the indicated approach is to increase the number of cells until the solution difference is less than a certain tolerance value, which for this report it is chosen at 1%. The **correctness** of the solution must be checked above all in the points where the flow has a critical behavior such as for example at the interface between two fluids (*Figure 4.8*) or in areas with high turbulence. In the figure is evident how for a coarse mesh the numerical diffusivity is higher, leading to a higher numerical error in the solution.
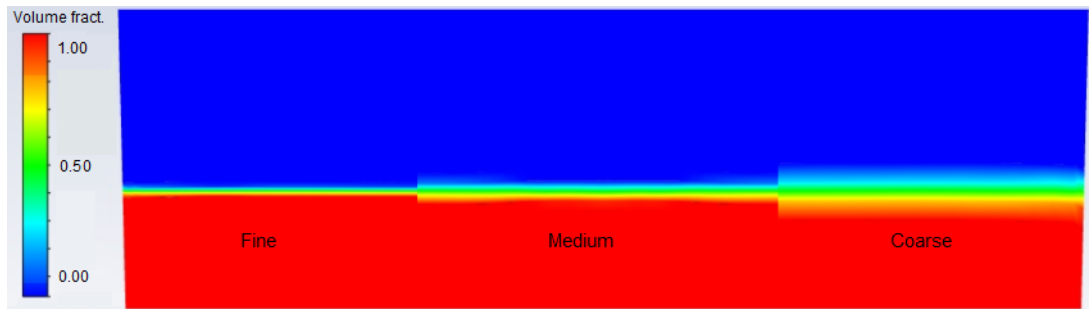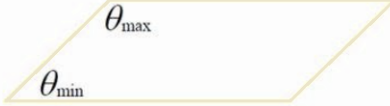
Figure 4.8: Volume fraction in a container with different mesh refinement

4.3.4 Mesh quality

Skewness: It is one of the primary quality measures for a mesh. A value of 0 indicates an equilateral cell (best) and a value of 1 indicates a completely degenerate cell (worst). In general the value should not exceed 0.85 [61]. A method to determine the skewness which applies to all cell and face shapes, based on the deviation from a Normalized Angle is given by the following formula, where θ_e is the equiangular face and its value is 60 for tets/tris and 90 for quads/hexas:

$$\text{Skewness} = \max\left[\frac{\theta_{\max} - \theta_e}{180 - \theta_e}, \frac{\theta_e - \theta_{\min}}{\theta_e}\right]$$

Aspect ratio: For generic triangles and quads is a function of the ratio between the longest side and the shortest side of the reconstructed quadrangles. The recommended values are: 100 where there is no strong transverse gradient (boundary layer) and <40 for the other area of the computational domain [62].

aspect ratio = 1   high aspect-ratio quad

Expansion ratio: Enables the mesh to be graded, or refined, in specified directions. It is the ratio of largest to smallest element volumes surrounding a node. For most of the cases is recommended a value lower than 1.2, otherwise significant computational error may happen.
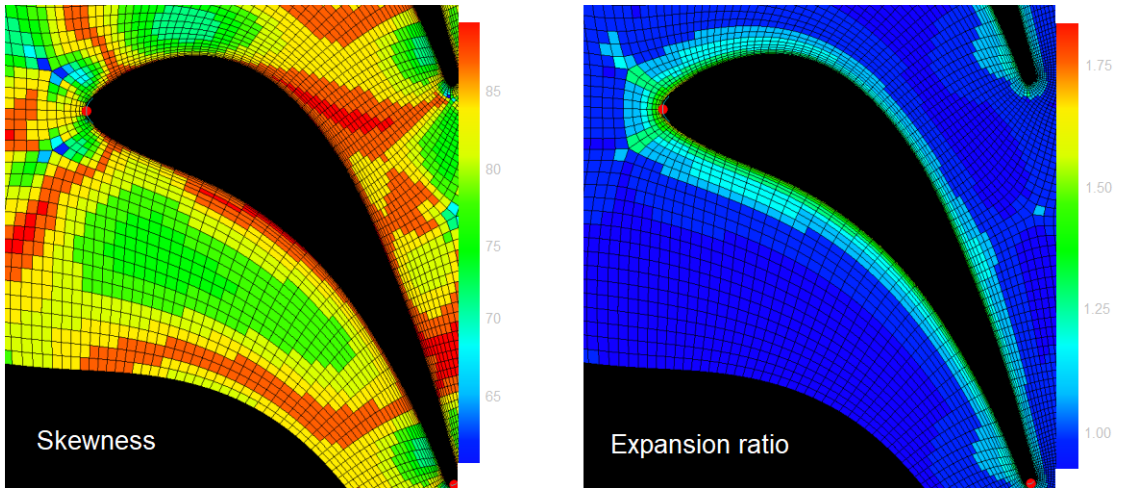
Figure 4.9: Skewness and expansion ratio: example from Autogrid User Guide

Chapter 5

Methodology

The main goal of the work in this thesis is to **evaluate performance** for a new gas turbine stage. The test turbine located in the Turbomachinery lab of the Heat and Power Department at KTH Royal Institute of Technology (Brinellvagen 68, Stockholm) has been in operation since 1989 for industrial and academic purposes. Currently, the test turbine is participating in a research project as a collaboration between KTH Royal Institute of Technology and Siemens Energy.

Many turbine components have remained the same over time such as: stator, hub, shroud and most of the measuring instrumentation. The component that has been changed is the **rotor blisk** which has a more advanced and innovative geometry. This new design is expected to lead to a reduction in aerodynamic losses and an improvement in performance compared to the previous one. In this report the new blisk is referred as test object No.6, Blisk 6 or Build 6 and the previous one is object No.5.

The evaluation of the performance will be done with a combination between CFD simulations and experimental tests. This **approach** has been increasingly used recently in the field of industrial design because of its effectiveness and reliability. For the experimental side the turbine facility and the measurement systems are firstly described. Following is shown the mesh generation process done using Autogrid5 and how to set the boundary conditions in ANSYS-CFX. Both tests will be conducted under the same **operating conditions**, in order to have homogeneous results comparable. Finally, the comparison of the performance of experiments and CFD and blisk 5 vs blisk 6, will be done graphically comparing the **efficiency** and **reaction degree** both in design operation and off design conditions.

For the **correct operation** of the turbine there are many other steps that were not performed for this report. In particular, the aerodynamic design is done by Siemens Energy AB (G.Schmidt, 2020) and the structural design by KTH (M.Guiterres Salas, 2021).

5.1 Why experiments and CFD?

Traditionally, both **experimental and analytical** methods have been applied for the study of fluid dynamics in order to understand the behavior of turbulent flows. Now the trend is to achieve more reliable results through the use CFD simulations, especially for industrial applications that require to achieve ambitious goals and product development in economically profitable times.

The **advantages of computational fluid dynamics** have been already listed in *Chapter 4*. Above all, the level of detail of the results is higher compare to the experimental approach. That's because in experimental tests only the points in the space with sensors are known and since they interfere with the fluid flow it is not possible to capture data from all the domain. On the other side for CFD analysis, which is based on approximated equations, there is a higher numerical error in the results. However, for its rapid and cost-efficient solution the use of this CFD has become fundamental especially in the early stages of the development.

Despite the great appraisal of CFD, there is no evidence that suggest a complete replacement of **experimental tests** by computational simulations in a short term period. It can be seen rather as a complementary approach that speeds up the initial stages of product development. One of the reasons why there is still a need of experiments is given by the limit of computers that are not, with the actual **computational capacity**, able to solve the governing equations directly (DNS).

Instead a more integrated approach between experiments and computational fluid dynamics is usually preferred. For the design of Blisk 6, CFD simulations and experiments have been combined following the underlying procedure:

1. *Simplified turbine model*: the geometry is built with a CAD tool and the performance is preliminary evaluated with CFD. By studying the velocity field of motion of the fluid, strategies can be found to minimize aerodynamic losses and have a potentially improved geometry compared to the previous ones.

2. *Detailed CFD model*: made introducing additional elements such as, the cooling circuit and a tip gap, to represent better the real system. Also the quality of the mesh is increased with refinement techniques.

3. CFD simulations and experimental trials in the laboratory are carried out with same operation conditions and the flow parameters are measured.

4. Validation of the CFD model with the results from experimental tests: if there is a difference in the results find other elements to introduce into the CFD model to make it as realistic as possible (iterate steps 2-4).

5. Check if there have been improvements in the performance compare to the previous blisk. Justify the results and find a direction for a new research.

6. Use the validated CFD model to simulate a new geometry design (step 1).

5.2 Experimental trials

The KTH Test Turbine facility is in operation since 1989 and was first described by Södergård et al. [26]. In particular in the Test section (see *Figure 5.1*), the turbine has interchangeable rotor and stator discs and can be equipped with up to three stages. New components are usually inserted there and their performance is evaluated and compared with the previous components.

5.2.1 Test facility

The air for the turbine is supplied by a 1 MWel air compressor with a maximum pressure of 4 bars and a nominal mass flow of 4.7 kg/s. The air flows through a cooler, a condensate water separator, mass flow orifice and then through a settling chamber before it enters the turbine. In *Figure 5.1*, it is possible to see the assembled test facility as during the test trials (on the left). When the Test section is open, the rotor and stator disc are visible, as shown in the figures on the right (above the stator and below the blisk rotor).

The inlet temperature can be set between 30°C and 70°C. The rotation of the turbine produces work which is evaluated through the **magnitude of the torque**, measured with a torque meter based on phase displacement between the two ends of a carefully calibrated torsion shaft. The turbine speed is controlled by variable fill hydrokinetic dynamometer (water brake), that had the additional function to dissipate the power produced in the turbine.
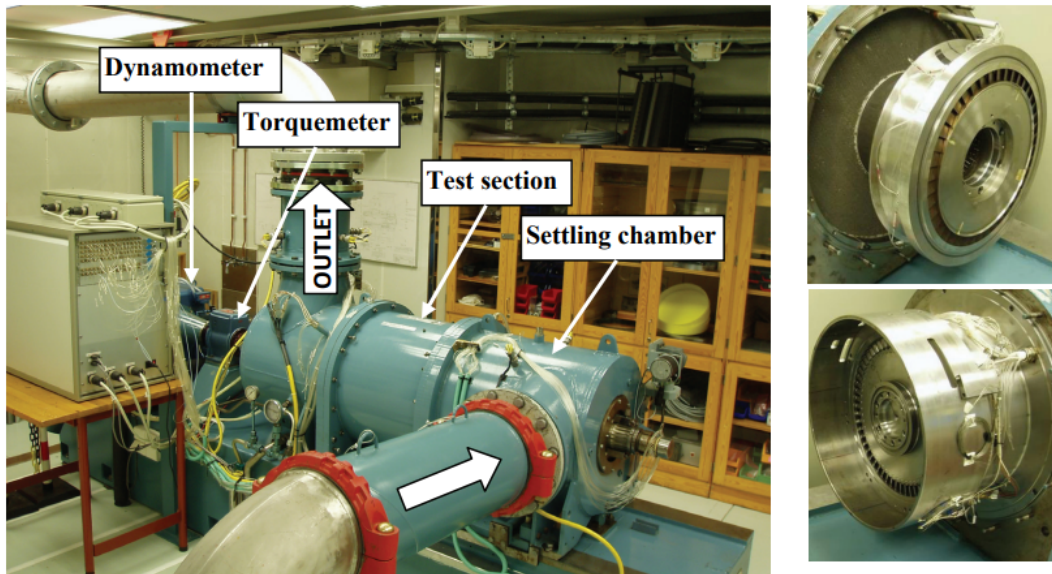
Figure 5.1: The test turbine facility and stator and rotor discs assembled

5.2.2 Description of the test objects

In the test section there are the stator and the rotor blisk of the turbine. To isolate the beneficial contribution of a new design, it is advisable to focus on one component at a time. In this study, the stator remains unchanged, while the object analyzed in detail is the **rotor disk**. The previous version, called object No. 5, has been replaced by object No. 6 (*Figure 5.2*), designed using performance improvement strategies, aiming above all at reducing aerodynamic losses. In particular it can be noted the introduction of two main loss reduction strategies:

- *Enwall contouring:* A endwall contouring has been applied to the blisk, obtaining a pronounced non-axisymmetric hub, which is expected to lead to a reduction in aerodynamic endwall losses. From the meridian view in *Figure 5.3*, it's possible to notice the aerodynamic shape of the hub of the rotor, compare to the one of the stator that has a traditional axisymmetric hub.

- *Reduced blade count* As shown in *Table 5.1*, the number of blades in the rotor had change from blisk 5 to blisk 6, decreasing from 60 to 49. Since near the surface of the blade there is high entropy generation, a reduction in the number of blades is expected to bring a benefit on the performance of the turbine and a reduction in aerodynamic losses. Moreover, there can be also a more global performance increase due to a reduction of the material/time utilized to build the blade and a decrease in the cooling flow rate, which can be used instead to power the turbine.

Figure 5.2: Rotor blisk of test object No 6
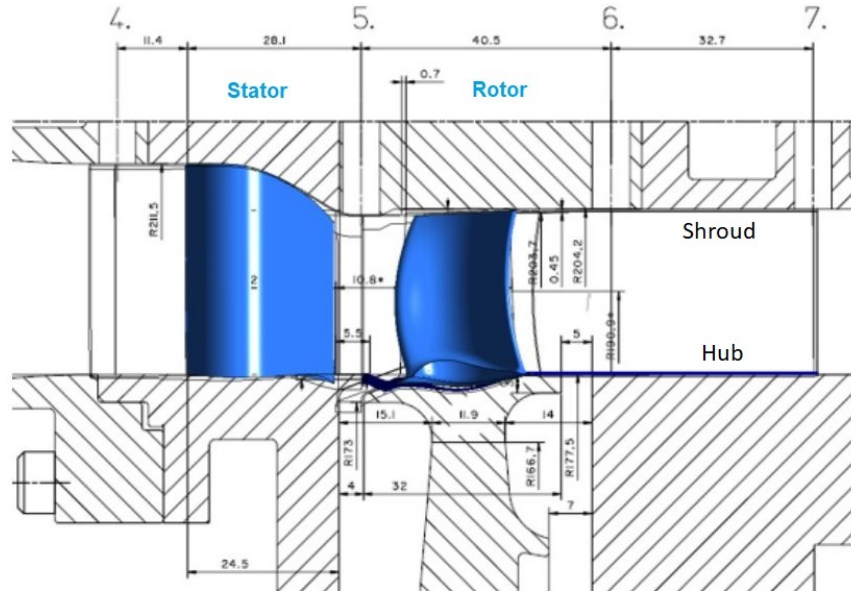
Figure 5.3: Cross sections of the test turbine

	Build 5		Build 6	
Parameter:	stator	rotor	stator	rotor
Hub radius, r_h [mm]	177.5	177.5	177.5	177.5
Diameter ratio, TE, d_h/d_t [-]	1.149	1.148	1.149	1.149
Pitch-chord ratio, t/b [-]	0.83	0.84	0.83	*1.08*
Aspect ratio, TE, h/b [-]	0.77	1.10	0.77	*1.16*
# of blades	42	60	42	49
tip clearance [mm]	-	0.40	-	0.40
Flow turning, γ_{mid} [°]	75.3	106	75.3	
Rotational speed [rpm]	-	10300	-	10500
Mach number, $Ma_{exit, rel}$ [-]	0.779	0.782	0.779	
Reynolds number, Re_{rel}, [-]	$6.9*10^5$	$3.7*10^5$	$6.9*10^5$	
Mass flow [kg/s]	3.47		3.49	
Pressure ratio, $\prod_{t-s}$ [-]	2.139		2.139	
Pressure based reaction degree, $\Lambda_{p,mid}$ [-]	0.389		0.389	
Flow coefficient, $\phi = c_a/U$ [-]	0.423		$0.54_{mid, TE}$	
Stage loading coefficient, $\psi = \Delta h_0/U^2$ [-]	1.368		1.30_{mid}	

Table 5.1: Selected geometrical and design parameters.

27

5.2.3   Measurement system

One of the most important parameters of a turbine is the stage efficiency that can be determined either thermodynamically, by measuring the values of temperature and pressure or **mechanically** using the mass flow, average pressure and temperature and shaft power. Generally, the enthalpy drop in the test turbine is small and the temperature measurements are sparse. Therefore, the efficiency based on total temperature drop is very sensitive to small changes in temperature and for these reason was decided to evaluate the efficiency by using mechanical parameters. In *Figure 5.4* the position of the main sensors is shown.

The first parameter used is the **torque** that is acquired with a torque meter. Following, the steady **pressures** are measured, with the atmospheric pressure as a reference, with a set of PSI9010 modules in appropriate ranges, which are re-zeroed pre- and post-measurements in order to check if there is a drift in the results. The absolute **temperature** is measured bt type-K thermocouples. A cold-junction unit with three PT100 resistive temperature sensors is used as temperature reference. Both pressures and temperatures are averaged over space and time. The sampling rate is 1 Hz. A standard orifice flange is employed for mass flow determination and calculated with formulas from ISO 5167-1 (1991) and ISO 5167-1, Amd.1 (1998). Uncertainties determined according to ISO/TR 5168 (1998). In *Appendix A* more details about the instrumentation and uncertainties of the measurements.
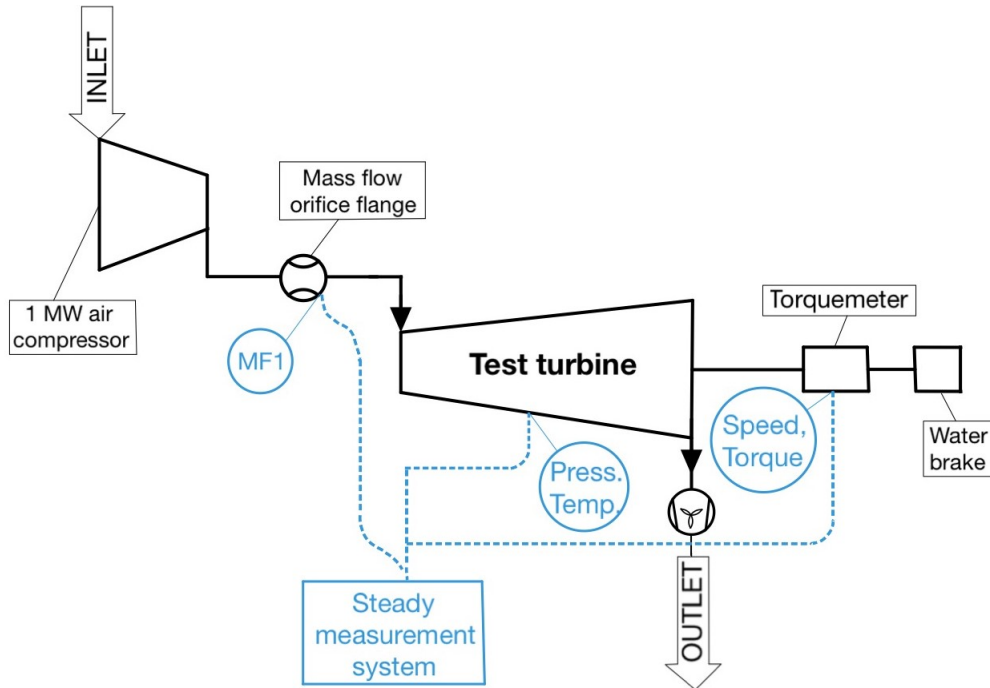
Figure 5.4: Layout of the measurement instrumentation

5.3 CFD simulations

In this section, it is explained how to obtain the same parameters measured in the experimental tests, through a CFD simulation. In this regard, two commercial softwares are used: for the mesh generation phase of the Numeca-AutoGrid5, while for the CFD simulation Ansys-CFX was used. The software Ansys-CFX offers a in built package for the generation of meshes in turbomachines called TurboGrid, but the results obtained with this method have not been satisfactory, for this reason the switch to Numeca-AutoGrid5.

5.3.1 Domain

It is well known that it is essential to save computational time in computational fluid dynamics. In *Chapter 4* it was explained how to decrease the number of nodes of the mesh with refinement techniques aimed at the most critical areas. Even before that there is a simpler method to reduce the mesh size, which is to exploit the geometry periodicity. In axial turbines it is possible to extract and analyze just a **section** and set periodic boundary conditions.

In the case of blisk 6, the rotor blisk is divided into 49 sections, of which only one is considered. The stator is instead divided into 42 parts, equal to its number of blades. Since the analysis is on the aerodynamics and not its mechanical resistance, the disk surface is neglected, selecting only the **blade** and the non axisymmetric hub. This also leads in a reduction of the computational domain. Moreover it should be noted, as shown in *Figure 5.5*, the section cut is not straight but follows the shape of the blade to avoid the splitting of the boundary layer.
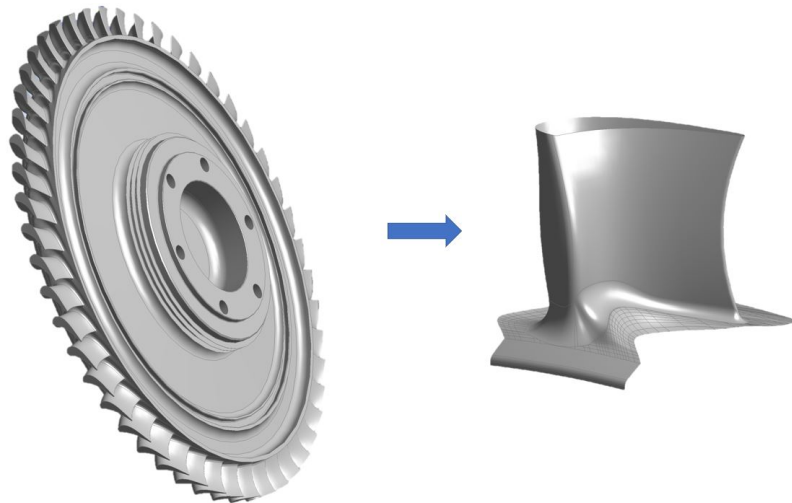
Figure 5.5: From CAD to CFD domain: entire rotor disc vs blade

5.3.2 Mesh 1: AutoGrid

In the next step, the mesh of the previously selected domain has to be generated. In addition to the blade itself, the mesh includes also the **flow path** and the air surrounding the blade. The inlet and outlet of the flow are placed far from the blade surface to have a more homogeneous distribution of speed, pressure and temperature where the boundary conditions are set.

During the mesh generation process, the most critical area to deal with has been the **non-axisymmetric hub**. The geometry was first imported ANSYS-CFX's mesh generation tool for turbomachinery components: TurboGrid. In the areas corresponding to the non-axisymmetric hub the reading of the geometry was incorrect leading to unsatisfactory results. For this reason it was chosen to use AutoGrid, which has implemented some of the refinements techniques discussed previously such as blocking, which leads to a good mesh quality even for the case of more complex geometries.

Geometry import

Before starting the mesh generation, in the solving procedure of the software there are two stages that have to be done manually by the user

1. Import the geometry of the blade from a CAD file.

2. Associate the elements of the geometry (lines or surfaces) with functional elements of the blade (blade, hub, shroud, non-axisymmetric hub, trailing edge, leading edge, meridian), as shown in the Figure 5.6.
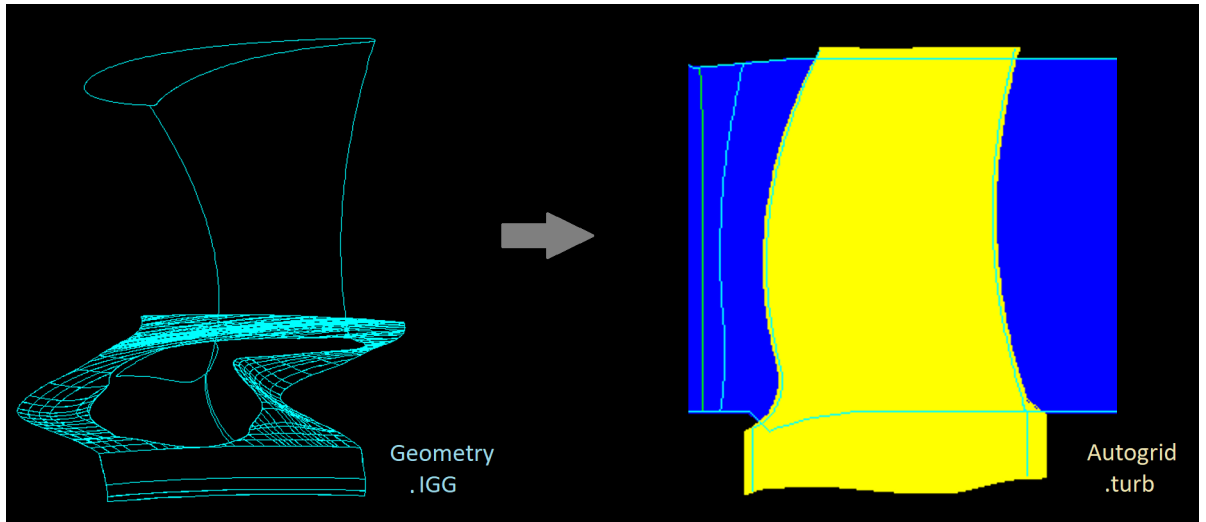
Figure 5.6: AutoGrid: from CAD to turbomachinery analysis

Errors

However, even in this case, importing such a complex geometry was not an easy process and some problems were encountered, which result in error messages from the software and inability to proceed with the mesh generation:

1. *Error in the selection of surfaces:* the current CAD file of the turbine geometry was not read correctly in the AutoGrid, preventing the selection of some surfaces. It was therefore replaced with another type of file.

2. *Error for no intersection between hub and leading edge*: caused by a small gap between the blade and the hub for tolerance reasons, it gave an intersection error between hub line and leading edge line. For this reason, the blade was lengthened with a CAD software until it passed the hub line in order to ensure the intersection with the leading edge.

3. *Meridian line generation error*: for the non-axysimmetric hub it was difficult to create the meridian line because it was formed by numerous surfaces each with its own meridian line. For this reason, first of all a larger surface was created made from the union of all the surfaces. But even in this case the meridian line created automatically in AutoGrid was wrong, so it was defined manually in CAD and then imported separately.

4. *Error due to discontinuity in the leading edge and trailing edge line:* by associating the edges between the suction side and pressure side of the blade with the leading and trailing edge, AutoGrid detected an error in the definition of these elements. This bug was solved by creating these lines in CAD and importing and associating them in AutoGrid as part of the turbine.

5. *Blade surface association error:* AutoGrid detected errors that are not entirely clear regarding the definition of the blade surface. Working again on the geometry file again in CAD, it was observed that there were multiple overlapping surfaces, leading to association errors in AutoGrid.

6. *Error in recognizing the interface between non-axisymmetric hub and blade.*

Most of these errors (1-5) were resolved with the above strategies after a long brainstorming process. After overcoming the errors due to the import of geometry and association of the blade elements, a rather basic mesh was generated for testing. The result was that there were no major problems in most of the domain, except in the interface area between the blade and the non-axisymmetric hub (6). Furthermore, for more details regarding the intermediate steps listed above, refer to Appendix B.1.
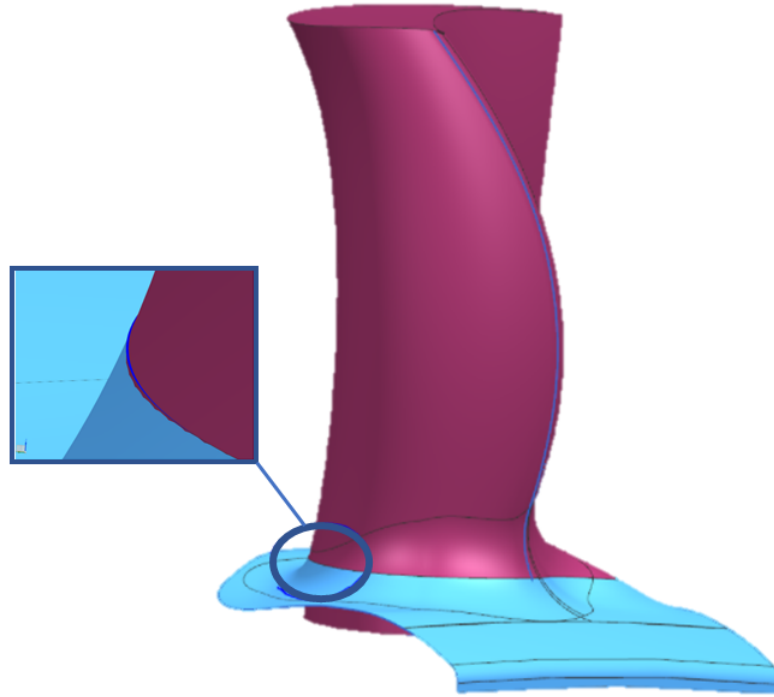
Figure 5.7: AutoGrid: negative cells position position

To solve this problem, the advice of a more specialized operator (Navid Navid Mikaillian) was requested in solving this problem who proposed two possible solutions:

1. Create a smoother blade-hub interface line in order to have a more gradual change of surface angle between blade and hub. This solution did not solve the problem (see Figure 5.7).

2. Divide the domain into three zones: stator, upper part rotor, lower part rotor containing also the non-axisymmetric hub. For the stator and the top of the rotor a mesh was generated in AutoGrid without any problems. For the lower part of the rotor, problematic in AutoGrid, the mesh will be generated with the ICEM program, by a specialized expert in this type of simulations (Mauricio Gutiérrez Salas).

5.3.3   Mesh 2: in AutoGrid + ICEM*

The purpose of a hybrid mesh with parts built in AutoGrid and parts generated in ICEM is primary to overcome the errors that result in AutoGrid when meshing the hub of the rotor. As has already been said, in the interface between blade and non-axisymmetric hub there is the presence of negative cells in the mesh and for which a suitable solution has not been found using AutoGrid. For this reason it was decided to use ICEM for that critical area (lower part of the rotor blade), while for the upper part of the rotor and for the stator the mesh was built in AutoGrid because of the rapidity and simplicity of meshing stardard geometries. A representation of the different domains mentioned above is shown in Figure 5.8.
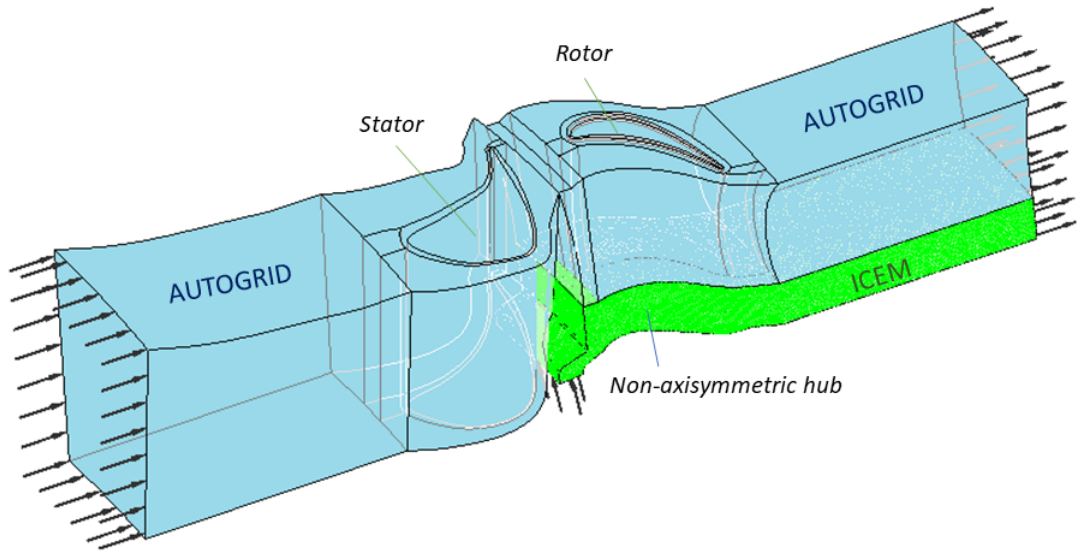
Figure 5.8: Mesh 3: the zones in AutoGrid and ICEM

The mesh generation in ICEM is more flexible and allows the solution of a large variety of geometries, but it also requires higher qualification. For that reason, the mesh generation in ICEM was made by Mauricio Gutiérrez Salas to speed up the mesh generation.

5.3.4 Boundary conditions definition

In order to set the **inlet** conditions, the section must be taken far enough away from the blades so as to not have an already turbulent region, due to the flow splitting on the blade leading edge. In the example in *Figure 5.9a* the velocity field is represented on XY planes at different z locations. Moving from the blade in negative z direction, the first plane with homogeneous conditions is z = -0.012m and that is closest plane to the blade on which the inlet conditions can be set. Usually they are taken a bit further as seen in *Figure 5.9b*. The same attention must also be given to the **outlet**, for which the turbulent phenomena are more intense (*Figure 5.9c*), therefore the first plane with homogeneous conditions it is even further for z = 0.12m.

One could evaluate the efficiency using the thermodynamic variables but, since this has not been done for the experimental tests results, it is preferred to use the exact same approach also for the simulations. This consists, in calculating the **torque** produced, rather than the enthalpy drop through the turbine.
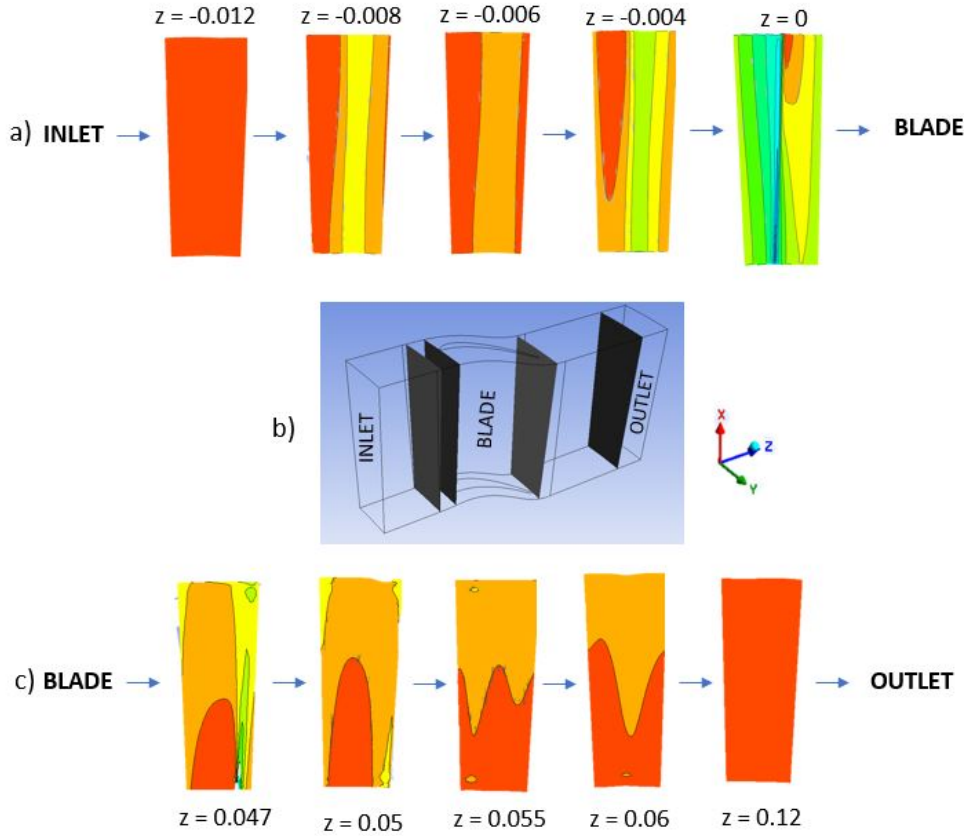
Figure 5.9: Velocity profile for different sections: a) inlet, b) 3D model, c) outlet.

5.3.5 Torque measurement

While for experimental tests the torque is measured with a torque meter based on a phase displacement between the two ends of a carefully calibrated torsion shaft, for CFD this evaluation takes place knowing the pressure distribution on the surface of the blade. The pressure difference between the suction side and pressure side allows rotation of the disk and it is called **blade loading**. In *Figure 5.10a* the mid-span pressure profile moving from the leading to the trailing edge is shown. Blade loading is an important aerodynamic design parameter in turbomachinery blades, it defines both the amount of work made, or extracted, by the blade and the distribution of such work from hub to tip/shroud.

However, the **torque** transmitted to the turbine shaft is often referred to. In order to calculate it, the pressure p is multiplied by a differential area dA and the lever r of the obtained force, integrating the result on the total area of the blade and hub. In more simple applications, the force on the hub is neglected, but being non-axisymmetric and three-dimensional, its contribution may be relevant. All this procedure it is actually done automatically in CFX by giving the total area on which the torque must be evaluated as an input to the software.
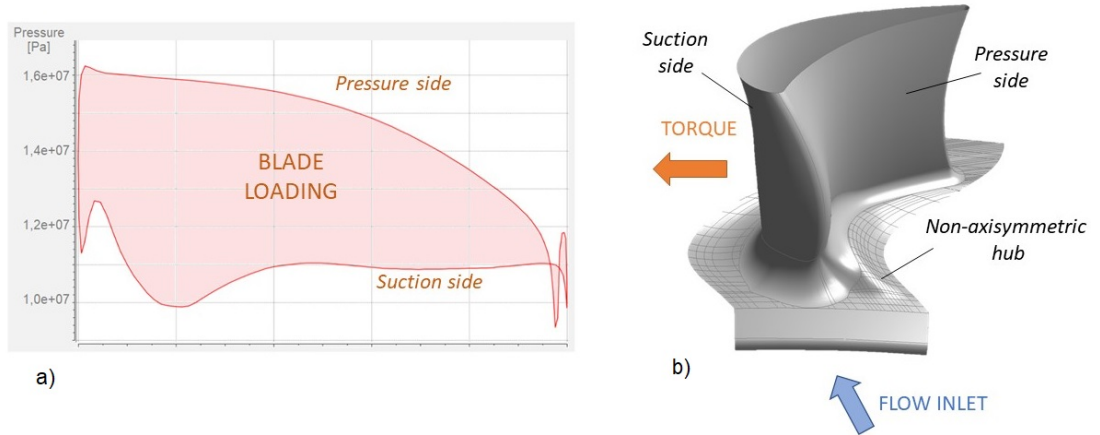
Figure 5.10: Blade loading (a) and blade sides (b)

In real turbines, often there is the presence of a tip gap and this contributes to a lower blade loading, that has a negative effect on the overall performance. However, the **tip gap** is inevitable because a tolerance between the blade tip and the casing must always be there for the correct operation of the turbine. In addition, as mentioned, to reduce the losses of viscous friction, the **number of blades** was reduced. For a constant value of the torque this means a higher blade loading. Whether this has really happened and what are the actual consequences on performance, will be analyzed later in the report.

5.4 Calculations: performance evaluation

In *Chapter 3.3* it has already been shown that there is a link between the variation of velocity and enthalpy and the production of work through Newton's second law of motion (Eq. 3.1) and the Euler equation (Eq. 3.4).

In this section the **efficiency** of the turbine is defined as an indicator of the performance of the turbine. Since it has been seen that speed triangles affect the work produced in the turbine, it is important to have some **non-dimensional parameters** to describe the kinetic characteristics of the incoming flow. Finally, it is used an effective graphical representation which consists the **maps** for the efficiency and degree of reaction. This will be the main tool for analyzing the results.

5.4.1 Turbine efficiency

Considering the **specific work** as the useful effect of the process, starting from the Euler Equation the formula 5.1 for the efficiency of the turbine is derived.

$$W = u_3 c_{3\theta} - u_2 c_{2\theta} = h_{01} - h_{03} \tag{5.1}$$

The **isentropic efficiency** is a common method to define the performance of a turbine. In this definition, the real enthalpy change (numerator) is compared with the one of an isentropic process (denominator). From the previous formula (Eq. 5.1) it have been shown that the two quantities can be expressed in enthalpy terms if the thermodynamic conditions at input and output are known:

$$\eta = \frac{h_{01} - h_{03}}{(h_{01} - h_{03})_{isentropic}} \tag{5.2}$$

A further step is to write the enthalpy difference $h_{01} - h_{03}$ as a function of the **turbine shaft torque**. However, the mechanical losses must also be included because they depend on the testing equipment and neglecting makes the results less of general use. Torque losses must therefore be measured and added to the torque shaft in order to have the actual work produced by the gas on the blade as follows:

$$\eta = \frac{h_{01} - h_{03}}{(h_{01} - h_{03})_{isentropic}} = \frac{\Omega(\tau_{shaft} + \tau_{losses})/\dot{m}}{(h_{01} - h_{03})_{isentropic}} \tag{5.3}$$

The use of the equation containing the torque (Eq. 5.3) is to be preferred to that with the variation of enthalpy (Eq. 5.2), as the the instruments to measure the torque have a greater **accuracy** than the ones for the evaluation of the enthalpy drop calculated through the thermodynamic conditions of the flow.

Total-to-total and total-to-static

As regards the denominator of the Eq. 5.2, the isentropic term can be written in terms of **total-to-static** or **total-to-total** efficiency. The definition to be prefered depends on whether the outlet stream rate is used later in another component or is wasted. In the first case, when the kinetic energy is exploited later, the total-to-total definition (Eq. 5.4) can be used. If instead the kinetic energy is lost, total-to-static efficiency (Eq. 5.5) is more appropriate. Another reason to use the first definition is when it is not possible to measure the outlet stagnation state.

$$\eta_{tot-tot} = \frac{h_{01} - h_{03}}{(h_{01} - h_{03})_{isentropic}} \tag{5.4}$$

$$\eta_{tot-stat} = \frac{h_{01} - h_3}{(h_{01} - h_3)_{isentropic}} \tag{5.5}$$

For limited temperatures the isentropic enthalpy drop can be calculated, considering the calorically perfect gas and with constant heat capacity. For the total-to-total definition it is therefore obtain from Eq. 5.6, while for total to static the static outlet pressure is used instead of the total one (Eq. 5.7).

$$(h_{01} - h_{03})_{isentropic} = c_p T_{01} \left(1 - \left(\frac{p_{03}}{p_{01}} \right)^{\frac{k-1}{k}} \right) \tag{5.6}$$

$$(h_{01} - h_3)_{isentropic} = c_p T_{01} \left(1 - \left(\frac{p_3}{p_{01}} \right)^{\frac{k-1}{k}} \right) \tag{5.7}$$

Normalized TS efficiency

For this report it is assumed that the analyzed stage is the last and for this reason it is calculated the **total-to-static** (TS) isentropic efficiency, while for the numerator, as already discussed, the equation for the **mechanical** evaluation of the enthalpy drop is used, in order to obtain greater accuracy of the results. The torque value is measured with the torquemeter for the experimental case and through the blade loading for the CFD simulation, as seen in the previous paragraphs.

Moreover, since it is a current industrial application, which must therefore be subject to a **privacy policy** regarding the results obtained, the efficiency value will not be defined in absolute value but relative. This allows to compare the efficiencies for the different cases analyzed: experimental vs CFD and object No.5 and object No.6. Normalization is done for all with respect to the same value which is the maximum of the efficiencies obtained in the analysis.

5.4.2 Non-dimensional flow parameters

To describe the motion of the fluid through the blades of an axial turbine, in alternative to the velocity triangle, it is possible to use non-dimensional parameters, among which the most common are the ones listed below.

The **flow coefficient** is the ratio between the axial speed c_x of the rotor and the blade speed u, as defined by Eq. 5.8. A high value of the flow coefficient indicates a preponderance of the axial component, while a low value indicates that the velocity has a large tangential component. For angles α tending to infinity, it is equal 1.

$$\phi = \frac{c_x}{u} = \frac{c_x}{\Omega r} \tag{5.8}$$

The **stage loading** can be defined as the ratio of the difference between tangential component of the absolute velocity through the rotor and the blade speed, as shown in Eq. 5.9. Using Euler's equation, Eq. 3.4, the kinematic term can be replaced with the corresponding values of total enthalpy obtaining a new definition of stage loading as the ratio between two for the total enthalpy drop, divided by the square of the rotation speed of the blade u.

$$\psi = \frac{2(c_{\theta 2} - c_{\theta 3})}{u} = \frac{2(h_{01} - h_{03})}{u^2} \tag{5.9}$$

The third parameter considered is the **degree of reaction**, and compares the acceleration through the rotor to the one in the entire stage. This can be expressed as a change of static enthalpy.

$$\Lambda = \frac{h_2 - h_3}{h_1 - h_3} \tag{5.10}$$

In the case of gas perfectly calorically, the specific heat c_p can be considered constant, thus being able to replace the enthalpies with the respective temperatures. Furthermore, if the process is assumed to be almost adiabatic and isentropic, the degree of reaction can be written as a function of the values of the pressures:

$$\Lambda_p = \frac{p_2 - p_3}{p_1 - p_3} \tag{5.11}$$

Another non-dimensional parameter for velocity is the **isentropic velocity ratio** ν. It is similar to stage loading, with the difference that the enthalpy drop is the total isentropic one and not the real one. The denominator is in fact equal to the speed that would be obtained by accelerating the flow isentropically from the inlet to the outlet conditions.

$$\nu_{tot-stat} = \frac{u}{\sqrt{2(h_{01} - h_3)}} \tag{5.12}$$

5.5 Operating points

Not all possible operating conditions are feasible in experimental tests and they may be restricted due to eventual prohibited operating windows set by the vibration analysis. Accordingly to the results in *Figure 5.11*, resonances from the tip-timing have been identified and for those regions is recommended to not run any experimental test. For high values of rotation speed the operating windows are pretty small. The test conditions at which performance is going to be evaluated both with experimental tests and through simulations, are listed in *Table 5.2*.
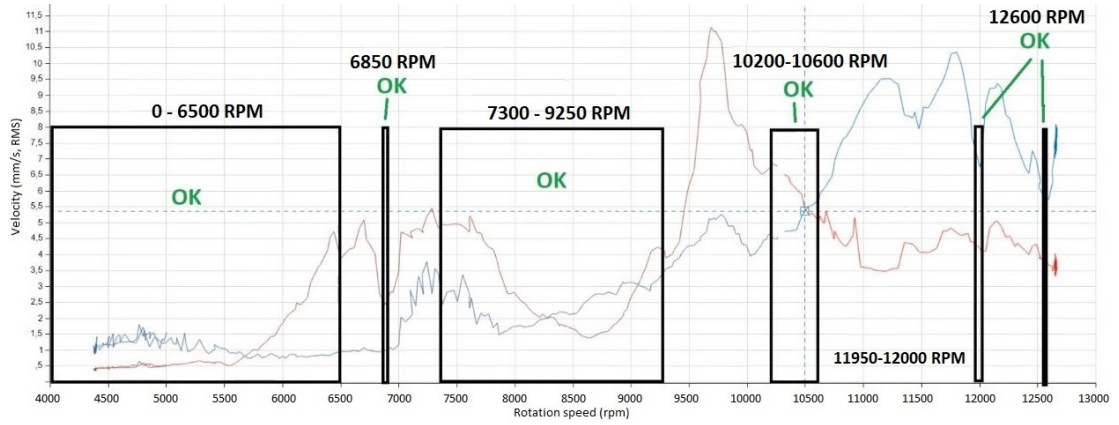
Figure 5.11: Results from vibration analysis

Inlet total temperature, t_{04} [°C]	70		
Pressure ratio, $\pi_{s\text{-}s}$ [-]	2.12		
Average mass flow [kg/s]	$3.5-3.6$		
O.P. Parameter:	N [rpm]	$v_{s\text{-}s}$ [-]	P [kW]
#6001	6500	0.3566	163
#6002	7300	0.4016	173
#6003	8300	0.4562	184
#6004	9250	0.5084	190
#6005	10250	0.5625	195
#6006	10400	0.5700	196
#6007	10600	0.5809	199
#6008	11950	0.6560	198

Table 5.2: Operating points

Chapter 6

Results

This section will illustrate the main results obtained from a global performance evaluation through experimental and simulation tests. The number of experiments sessions varied according to the upcoming results. Using the instrumentation and procedures described previously in the section dedicated to the Methodology, the trials sessions can be summarized as following:

1. **Experimental tests:** measurements were carried out in the laboratory of the Unit of Heat and Power Technology the Royal Institute of Technology (KTH) and the data were analyzed in a programmable file in Excel. The data was collected for both blisk 6 and blisk 5 and analyzed with the same methodology. There have been two measurement sessions for blisk 6: one in December 2021 called Blisk 6 (2021) and one in January 2022 called Blisk 6 (2022). The difference in operating conditions between the two tests will be discussed later. Similarly, a performance trial has been carried out also for blisk 5, refered to as Blisk 5 (2022).

2. **CFD simulations:** After performing the experimental tests, the same operating conditions measured in the real turbine, through the experiments, are implemented for the CFD simulations. The mesh used is Mesh 2 previously discussed (AutoGrid + ICEM).

The efficiency values, calculated using the data measured from the experimental tests have been elaborated in order to compare first of all the blisk 6 with respect to the previous blisk 5, expecting an improvement in performance given the suggestions from the theory. After that the experimental results are compared with those of the CFD simulations. In this case the expected result is similar values of the efficiency for the experiments and simulations.

In both cases the results are not perfectly aligned to the expectations. Some reasons for this behaviour are given in the section "Discussion" (Chapter 6.5).

6.1 Experiments: global performance

6.1.1 Blisk 6 (2021)

In carrying out the first experimental tests, the rotation speed was varied between 6000 and 11950 rpm considering, as previously mentioned, to take into consideration the accessible areas defined by tip-timing analysis. On the other side, the values of the pressure ratio, outlet pressure and mass flow values were kept constant. This allowed to compare the results, highlighting the influence of the rotation speed on the resulting efficiency and degree of reaction.

The pressure ratio was therefore set at 2.12, the outlet pressure at 104700 Pa and the mass flow around 3.6 kg/s. Observing the measured values, shown in Figure 6.1, the constrains on the pressure conditions are met.
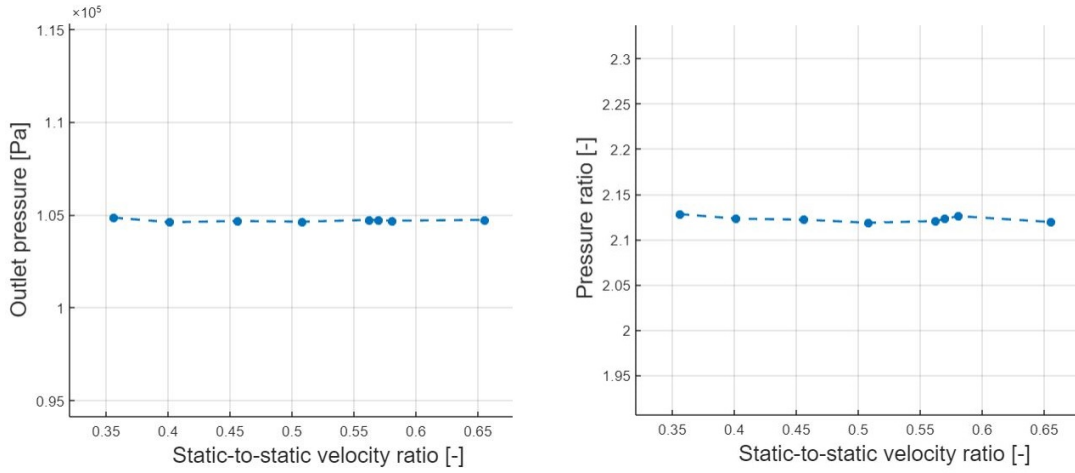
Figure 6.1: Experiments blisk 6 (2021): outlet pressure (a) and pressure ratio (b)

In Appendix C.1 other characteristic parameters of the turbine such as the rotation speed, the mass flow and the extracted power have been checked. No evident irregularities were found in these measurements.

This first set of experiments was useful in order to understand if the instrumentation was working correctly and if the results obtained were reasonable. However, they are not as significant in order to compare the Blisk 6 with the Blisk 5, because the only value common to both tests is the pressure ratio, while other variables were not checked yet. A more in-depth research of the operating conditions used for Blisk 5 (2019) was therefore carried out.

6.1.2   From Blisk 6 (2021) to Blisk 6 (2022)

The data from the experimental measurements on Blisk 5 for a previous research in 2019 was found and analyzed. What emerged is that some operating conditions are different from those set for the experimental trials on Blisk 6 (2021). In order to correctly compare the results of blisk 6 with those of blisk 5, some operating conditions must be restored so as to be homogeneous for the two cases:

1. *Turbulence grid*: changed in the period between measurements on blisk 5 (2019) and blisk 6 (2021). For the new measurements on blisk 6 (2022), the previous one had be restored.

2. *Mass flow and turbine constant:* there is a small deviation in their values which, however, could have a large impact on the results (see *Figure 6.2*.

3. *Outlet pressure*: in both cases the value is approximately constant but it is not the same. For blisk 6 (2021) it is around 104700 Pa and for blisk 5 (2019) it is around 103300 Pa. In the next test a value of around 103300 Pa will also be imposed for blisk 6.

4. *Torquemeter calibration constants*: there had been a variation of the working characteristics of the torquemeter which might have influenced and changed also his calibration curve.
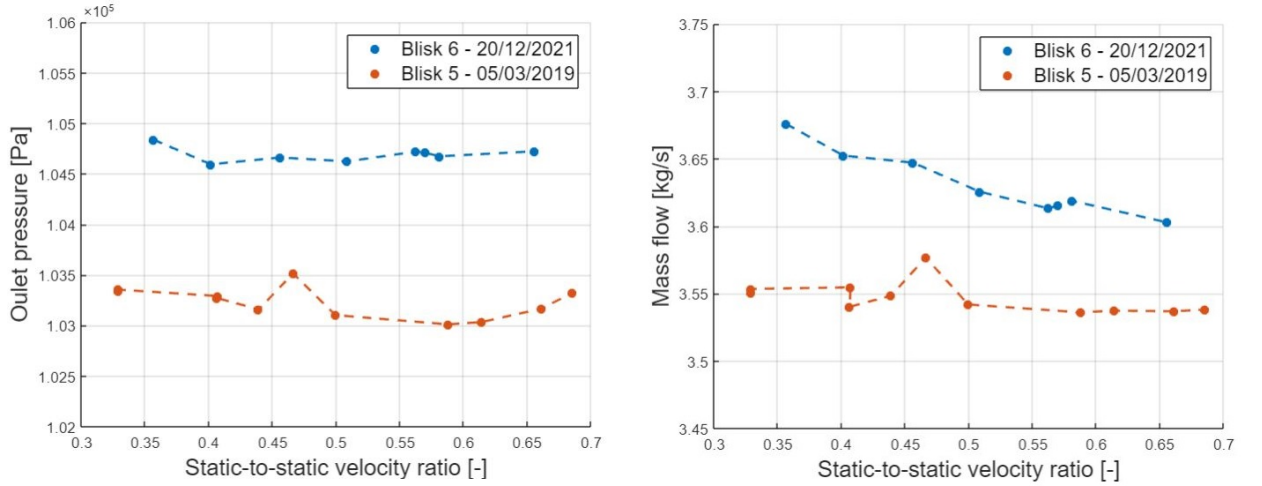

Figure 6.2: Blisk 6 (2021) and Blisk 5 (2019): Outlet pressure and Mass flow

6.1.3   Blisk 6 (2022)

For the new experimental tests the following changes were therefore made:

- The turbulence grid was changed;

- The outlet pressure is set at 103300 Pa.

The pressure transducers for the flow rate were also reset to obtain more accurate results. The values obtained with the new conditions are shown in Figure 6.3: the values measured for blisk 6 (2022) and blisk 5 (2019) as regards mass flow and outlet pressure, are pretty close to each other.
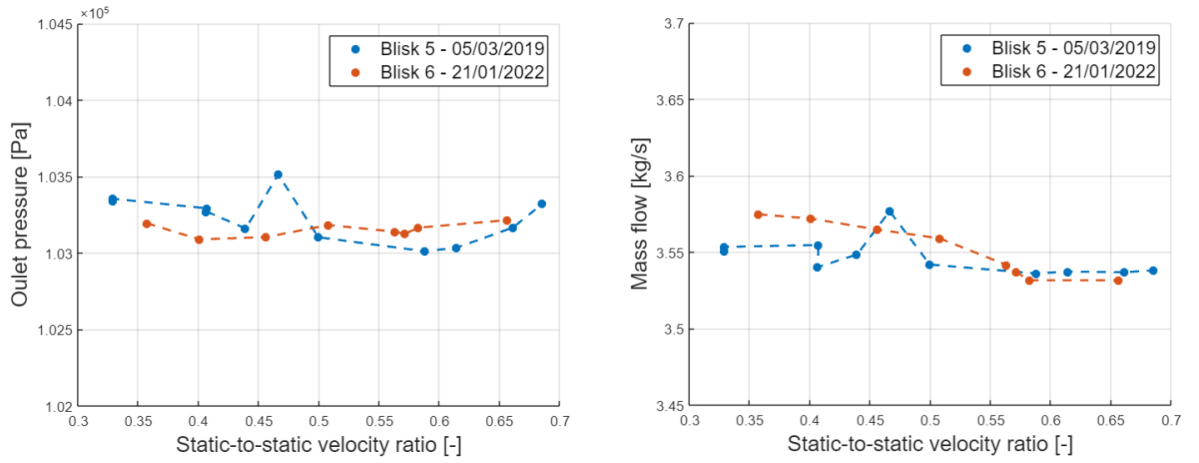
Figure 6.3: Blisk 6 (2022) and Blisk 5 (2019): Outlet pressure and Mass flow

6.1.4   Blisk 5 (2022)

With the above mentioned procedure the boundary conditions of the two tests (blisk 5 (2019) and blisk 6 (2022)) were homogenized (point 1-3 of the previous list). However, concerning measuring instrumentation, that might have changed the type of operation (eg calibration curve). For this reason it was considered appropriate, for a total homogeneity of the results, to repeat the measurements for blisk 5, naming this last test Blisk 5 (2022). In this way it's more reliable to compare the two components, limiting the factors related to the operating conditions.

The operating points for blisk 5 are different from those of blisk 6 since the results from the tip-timing for this turbine were different. The operating points for blisk 5 have been set at: 6500, 7300, 8300, 9400 , 10200, 10500, 11930, 12350 and 12600 rpm.

6.2   Comparison: Blisk 6 vs Blisk 5

As a comparison parameter for the performance, the formula of efficiency using the torque and the degree of reaction calculated with the pressures is used . The results obtained are shown in Figure 6.4 and Figure 6.5. The curves of the efficiencyfor blisk 6 and blisk 5 are overlaped which is a less positive result than predicted by the theory. While the degree of reaction deffers slightly for low velocity ratios. A possible explanation of the results will be given in *Chapter 6.5*.

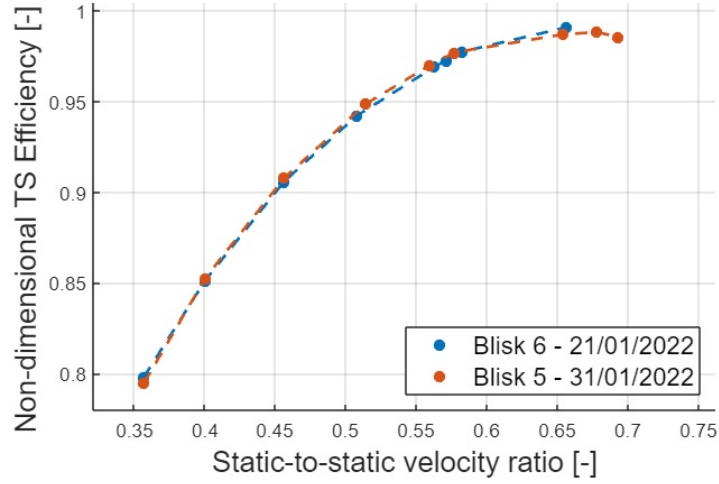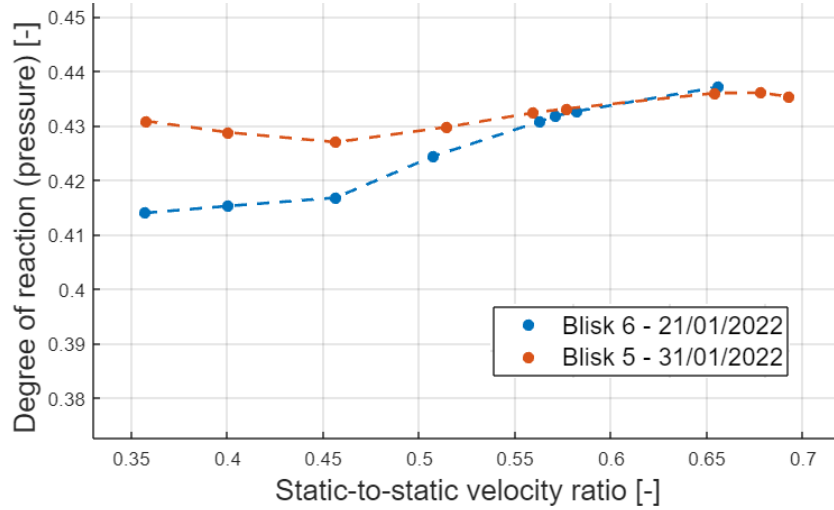**Figure 6.4:** Blisk 6 and Blisk 5 (2022): Non-dimensional Efficiency Total-to-static

Figure 6.5: Blisk 6 (2022) and Blisk 5 (2022): Degree of reaction

44

6.3   Simulations

The boundary conditions measured in the experimental tests and set in the simulations are: total inlet pressure, total inlet temperature, static pressure outlet. As a first approximation, a constant value was set over the entire surface of the inlet or outlet, making sure, as previously mentioned, that the section is far enough away from the blade not to include areas that are already highly turbulent. However, in the experimental tests the measurements were taken very close to the surface of the blade, therefore it is necessary to ensure that by setting homogeneous boundary conditions on the surface of the inlet (IN) and outlet (OUT), the values measured in the experimental tests were reached to the sections S4 and S7. This was verified for all simulations using an iterative method for some cases.
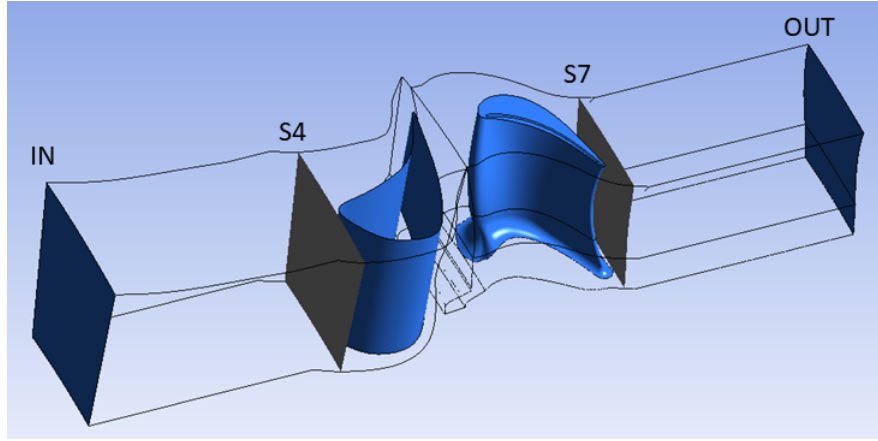
Figure 6.6: Simulation: boundary conditions sections

6.4   Experiments vs simulations

After that the boundary conditions are correctly posed, two of the most fundamental parameters that contribute to the calculation of efficiency are measured: mass flow and torque. As can be seen in Figure 6.7, the trend of the curve for the experimental tests and for the simulations are similar but their value is different by an approximately constant value. This also transmits to the efficiency where the experimental efficiency is higher than the simulations one 6.8 with an approximately constant difference between the two efficiencies. Also in this case the results seem different from what was expected: in fact, in the experiments there is the presence of some losses linked for example to the friction between the machinery, which does not happen in the experimental tests in which these losses are zero. A possible explanation of this effect is given in Chapter 6.5.
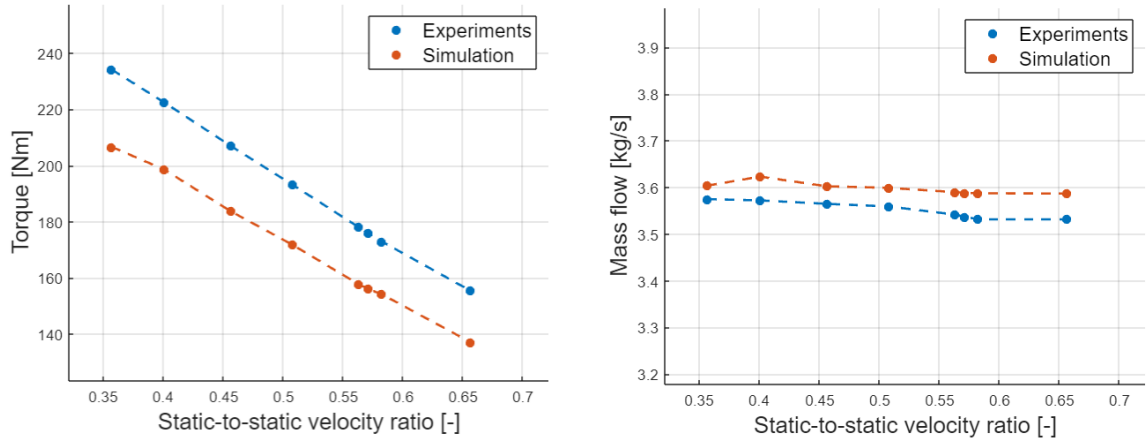
Figure 6.7: Simulations and experiments: Torque and Mass flow
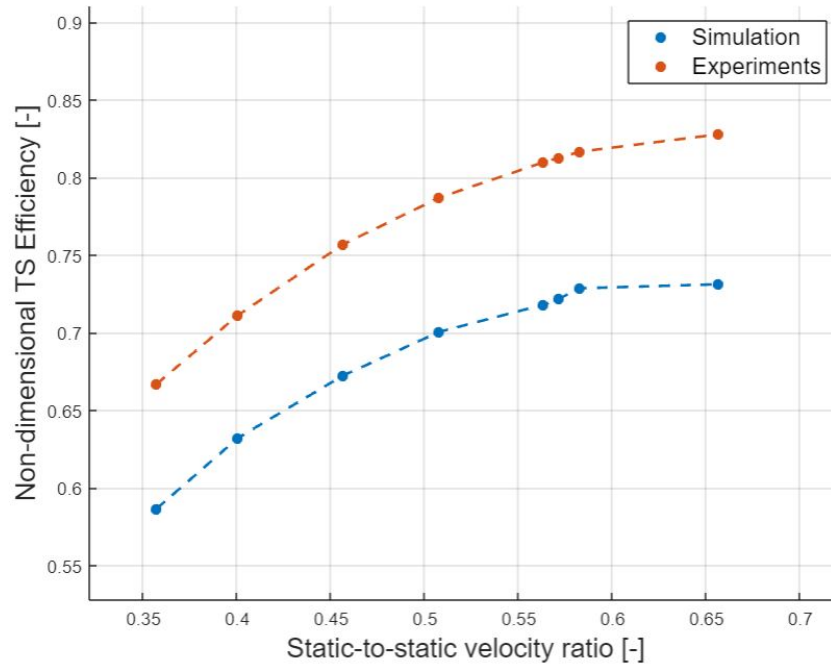
Figure 6.8: Simulation and experiments: TS Efficiency

6.5 Discussion

As previously mentioned, the results obtained in the comparison of blisk 5 and blisk 6 differ from what was expected based on the Literature review. Even for the simulations the results are quite far from what was expected. Therefore, some explanations are given in this chapter of what may be the cause of these discrepancies. This should indicate that the intensity of horseshoe vortex and turbulent mixing between the mainstream and coolant has decreased.

6.5.1 Blisk 5 vs Blisk 6

With the addition of a non-axisymmetric hub with endwall contouring, a decrease in losses due to secondary losses was achieved in other studies [39, 40, 41, 42], leading to an increase in efficiency. In the case, analyzed there were no such evident benefits. The reasons for this effect could be:

1. *Secondary losses have been reduced by endwall contouring, but there are additional losses due to other causes, including for example:*

   a. The non-axisymmetric hub takes a larger volume than a simple one and acts as an obstruction for the mainstream creating more aerodynamic losses (see *Figure 6.9*).
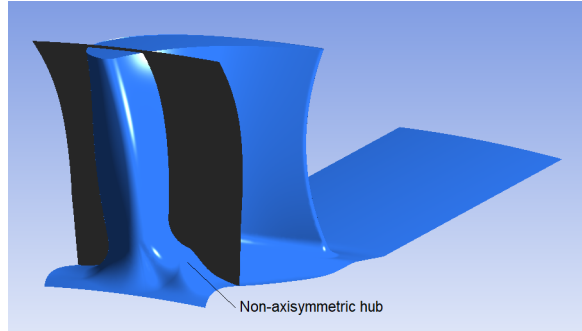
Figure 6.9: Non-axisymmetric hub shape

2. *Secondary losses were not significantly reduced with endwall contouring.*

   a. The secondary losses were not very significant and therefore a decrease does not affect the final result.
   b. Endwall contouring was not enough to reduce these losses.

To investigate these hypotheses more in depth, it would be necessary to have the results of the simulations on blisk 5, which are not available and, for reasons of time, it was not possible to repeat them.

6.5.2 Experiments vs Simulation

In the course of this report, an attempt has been made to suggest and reproduce rather similar operating conditions between experiments and simulations. The ideal result would be that of overlapping curves between experiments and simulations so as to reproduce the tests in the laboratory on the computer, speeding up research times. However this is very difficult to achieve while setting the same boundary conditions due to inherent differences of the two methods:

- The numerical simulations are based on approximations of the governing equations, therefore there is always a numerical error.

- There are additional losses in experiments related to the actual operation of the machinery, which are not considered in the calculations.

- In numerical simulations a conservative method is used to calculate aerodynamic losses, which are overestimated, leading to a reduction in efficiency.

Furthermore, despite the attention paid to researching and defining the value and position of the boundary conditions, some simplifications have been made with the methods described above. This happened due to the long period it took to solve all the problems related to the mesh generation described above. A satisfactory mesh was obtained only at the end of the performance study period so there was not much time left to do very elaborate simulations. Some of these simplifications are listed below and may have affected the final result:

- The boundary conditions were assigned as homogeneous over the entire surface of the inlet and outlet. In reality this does not happen because it is more likely that they are either more turbulent flows, or at least a profile that varies near the walls.

- Total pressure inlet and static pressure at outlet have been set. This means that the procedure was iterated only to obtain the correct outlet pressure, as explained above. The total pressure is conservative in the area before the blade, so it was easy to set it equal to the measured total pressure. However, from the experimental tests there are more measurements of the static pressure than of the total one, therefore it would be more correct to set the one with an iterative procedure similar to that for the outlet.

Since there is a much larger difference than expected between experiments and simulations, the static pressure in the inlet were measured to understand if the difference between that of the experiments is actually so great as to justify the difference it the efficiency value. However, this is not the case. The difference between the static pressure values is less than 1% (see Appendix C.2) so this is not enough to justify such a low efficiency in simulations.

Chapter 7

Conclusions

In this chapter the main parts of this thesis work will be summarized, the most relevant results, the future work that is needed to further complete the results obtained and the impact of the research, especially with regard to sustainability.

7.1 Main sections of the work

This thesis work contributed to the study of the overall performance of a new component of a gas turbine: the rotor blisk. The goal was to be achieved with experimental tests and numerical simulations. Some of the main activities have overlapped or have been carried out in parallel, but some main phases can be identified as following:

- *Literature review:* which helped to form a deeper background knowledge and an expectation on the results to be obtained. From reading studies on the introduction of non-axisymmetric hubs and endwall contouring, expectations went in the direction of an improvement in the efficiency of the current blisk (blisk 6) compared to the previous one (blisk 5).

- *Mesh generation:* it was the longest and most complex phase, due to problems reading geometry by the mesh generation softwares. This happened because the presence of non-axisymmetric hubs was not correctly read by TurboGrid before, and also AutoGrid after (Mesh 1), leading to all the errors previously described. Therefore, we finally opted for a more complex strategy, which sees some areas with mesh created in AutoGrid and the rotor hub area created in ICEM (Mesh 2). This phase required a great amount of time and resources.

- *Experiment trials:* This phase was postponed due to delays in the installation of the turbine due to external events. Despite this, three experimental test

sessions were still carried out: two on the new blisk, called blisk 6 (2021) and blisk 6 (2022) and a test on the old blisk, called blisk 5 (2022).

  – The first test was useful to verify the correct functioning of the instrumentation for experiments and measurements.

  – The second was more accurate in setting the operating conditions so as to have a comparison more on par with the blisk 5, setting the same pressure ratio and the same pressure at the outlet, also obtaining a similar massflow as for the tests on blisk 5 (2019).

  – Finally, the test for blisk 5 was repeated to make sure to have absolute homogeneity in the data collection procedure.

- *Simulations:* Numerical simulations were carried out using the CFX software, specific for fluid dynamics analysis for turbomachinery. The same boundary conditions as those measured in the experimental tests, both for total and static pressure, were reproduced through an iterative method.

7.2   Summary of the results and Future work

The results obtained were different from what was anticipated by the literature review and therefore gave rise to a more in-depth discussion of the results:

- *Blisk 5 vs blisk 6:* The difference between the two is less marked than imagined. The most plausible cause that has been found is that endwall contouring reduces secondary losses, but at the same time the non-axisymmetric wall acts as an additional obstruction by locally increasing aerodynamic losses. It would have been useful to test these hypotheses through a comparison with the numerical simulations on blisk 5, comparing the dynamics of the flow with that of the blisk 6, for example by looking at the velocity field.

- *Experiments vs simulations:* The efficiency achieved with the simulations was much lower (around 10% less). This is a very low result that is difficult to explain with numerical approximation errors or due to the use of homogeneous profiles for boundary condions. Again it would be necessary to go deeper in the search for the causes, but this was not possible in this report because a lot of time was spent for the generation of the mesh.

In addition to a more in-depth research of this specific turbine, which will be continued within the research group, it is important to work for a continuous improvement of this type of turbines, given the great environmental impact that also has a small improvement in their efficiencies, as has been said and supported by scientific articles in the initial chapters of this report.

Author

Claudia Florentina Balan
Double Degree Programme in Vehicle Engineering (Sustainable Energy)
Politecnico di Torino, KTH Royal Institute of Technology

Place

Heat and Power Department of KTH Royal Institute of Technology
Brinellvägen 68, Stockholm, Sweden

Supervisors

Mirko Baratta
Professor at the Department of Energy
Politecnico di Torino

Jens Fridh
Researcher at the Division of Heat and Power Technology
KTH Royal Institute of Technology

Mauricio Gutiérrez Salas
Researcher at the Division of Heat and Power Technology
KTH Royal Institute of Technology

Navid Mikaillian
Industrial Supervisor
Siemens Industrial Turbomachinary

Bibliography

[1] D Winterbone and A Turan. *Advanced Thermodynamics for Engineers*. eng. Second edition. Oxford: Elsevier Science Technology, 2015. ISBN: 9780444633736 (cit. on p. 1).

[2] Pasquale M Sforza. *Theory of Aerospace Propulsion*. eng. Oxford: Elsevier Science Technology, 2011. ISBN: 1856179125 (cit. on p. 1).

[3] Arturo Benito and Gustavo Alonso. *Energy Efficiency in Air Transportation*. eng. Saint Louis: Elsevier Science Technology, 2018. ISBN: 9780128125816 (cit. on p. 1).

[4] William C. Strack. «General aviation turbine Engine (GATE) Overview». In: (1983) (cit. on p. 1).

[5] Stephen Pope. «Piston Engine Aircraft Technology». In: (2012) (cit. on p. 1).

[6] Doug Woodyard and Malcolm Latarche. *Pounder's Marine Diesel Engines and Gas Turbines: And Gas Turbines*. eng. Oxford: Elsevier Science Technology, 2009. ISBN: 0750689846 (cit. on p. 1).

[7] Claire Soares. *Gas Turbines: A Handbook of Air, Land and Sea Applications*. eng. Second edition. Oxford: Elsevier Science Technology, 2014. ISBN: 0124104614 (cit. on p. 1).

[8] Paul Breeze. *Power Generation Technologies*. eng. San Diego: Elsevier Science Technology, 2019. ISBN: 0081026315 (cit. on p. 1).

[9] Aftaniuk V. «Analysis of gas flows in ships turbines». eng. In: *Scientific Bulletin ("Mircea cel Bătrân" Naval Academy)* XXII.1 (2019), pp. 318–322. ISSN: 2392-8956 (cit. on p. 1).

[10] International Energy Agency (IEA). «Global Energy Review: CO2 Emissions in 2020». In: (2020) (cit. on p. 1).

[11] The International Council on Clean Transportation (ICCT). «CO2 Emissions from commercial aviation: 2013, 2018, 2019». In: (2020) (cit. on p. 1).

[12] World Nuclear Association. «Carbon Dioxide Emissions from Electricity». In: (2021) (cit. on p. 1).

[13] A.J.A Mom. *1 - Introduction to gas turbines*. eng. Elsevier Ltd, 2013, pp. 3–20. ISBN: 0857096060 (cit. on pp. 1, 3).

[14] Simons Boiler Co. «Cogeneration Systems - Combined Heat Power». In: (2021) (cit. on p. 2).

[15] U.S. Department of Energy Efficiency and Renewable Energy. «Combined Heat and Power Technology Fact Sheet Series». In: (2016) (cit. on p. 2).

[16] Paul Breeze. *Gas-Turbine Power Generation*. eng. San Diego: Elsevier Science Technology, 2016. ISBN: 9780128040058 (cit. on p. 3).

[17] Center for Climate and Energy Solutions. «Technology Solutions: Natural Gas». In: (2021) (cit. on p. 3).

[18] MET Group. «Natural Gas vs Coal - Environmental Impact». In: (2021) (cit. on p. 3).

[19] Jens Fridh. *Experimental Investigation of Performance, Flow Interactions and Rotor Forcing in Axial Partial Admission Turbines*. eng. Trita-KRV. 2012. ISBN: 9175012243 (cit. on pp. 3, 61).

[20] Seong Won Moon and Tong Seop Kim. «Simulation of Optimizing the Partial Load Performance of a Gas Turbine Combined Cycle Using Exhaust Heat Recuperation and Inlet Bleed Heating». eng. In: *Journal of engineering for gas turbines and power* 143.6 (2021). ISSN: 0742-4795 (cit. on p. 3).

[21] José Carlos Dutra, Maria Angélica Gonzalez Carmona, Andrés Felipe Lazaro Alvarado, and Alberto Coronas. «Modeling of a Cogeneration System with a Micro Gas Turbine Operating at Partial Load Conditions». eng. In: *Journal of sustainable development of energy, water and environment systems* 5.2 (2017), pp. 139–150. ISSN: 1848-9257 (cit. on p. 3).

[22] Andreas Poullikkas. «An overview of current and future sustainable gas turbine technologies». eng. In: Renewable and Sustainable Energy Reviews 9.5 (2005), pp. 409–443. ISSN: 1364-0321 (cit. on p. 4).

[23] M Schnieder and T Sommer. *6 - Turbines for industrial gas turbine systems*. eng. Elsevier Ltd, 2013, 188, 224e–223, 224e. ISBN: 0857096060 (cit. on p. 4).

[24] Steven E. Kuehn. «Advancing gas turbine technology: evolution and revolution». In: (1995) (cit. on p. 4).

[25] Pankaj Bajaj, Fulvio Magni, and Peter Flohr. «A Performance Upgrade of an Industrial Gas Turbine Based on Additive Manufactured Components». In: Sept. 2020, pp. 500–509. ISBN: 978-3-030-54333-4. DOI: `10.1007/978-3-030-54334-1_35` (cit. on p. 4).

[26] Söderberg O. Södergård B. Henriksson K. «Turbine testing facility - Technical Report, TRITA-KRV-1989-03; ISSN 1100- 7990; Department of Thermal Engineering, The Royal Institute of Technology, S-100 44 Stockholm, Sweden». In: () (cit. on pp. 6, 25).

[27] Autogrid5. «http://www.parsmakina.com/en/product/autogrid5/». In: () (cit. on pp. 6, 19).

[28] Ansys CFX. «https://www.ansys.com/products/fluids/ansys-cfx». In: () (cit. on p. 6).

[29] Marzano Mario Rocco. «Appunti di Fondamenti di macchine del corso di Ingegneria Energetica (2018)». In: () (cit. on pp. 7, 10).

[30] J. D. Denton. «Loss Mechanisms in Turbomachines». In: Turbo Expo: Power for Land, Sea, and Air Volume 2: Combustion and Fuels; Oil and Gas Applications; Cycle Innovations; Heat Transfer; Electric Power; Industrial and Cogeneration; Ceramics; Structures and Dynamics; Controls, Diagnostics and Instrumentation; IGTI Scholar Award (May 1993). V002T14A001. DOI: 10.1115/93-GT-435. eprint: https://asmedigitalcollection.asme.org/GT/proceedings-pdf/GT1993/78897/V002T14A001/4457435/v002t14a001-93-gt-435.pdf. URL: https://doi.org/10.1115/93-GT-435 (cit. on pp. 11, 12).

[31] Ning Wei. *Significane of loss models in aerothermodynamic simulation for axial turbines.* eng. Trita-KRV. 2000. ISBN: 9171705406 (cit. on p. 11).

[32] J.D. Denton. *Loss Mechanism in Turbomachines.* eng. 1993 (cit. on p. 11).

[33] O. Zweifel. *Die Frage der optimalen Schaufeteilung bei Beschaufelungen von Turbomaschinen insbesondere bei grosser Umlenkung in der Schaufelreihen.* ger. 1945 (cit. on p. 11).

[34] Hongkai Yang, Weihao Zhang, Zhengping Zou, Shaowen Zhang, Fei Zeng, and Wenqi Xu. «The Development and Applications of a Loading Distribution Based Tip Leakage Loss Model for Unshrouded Gas Turbines». eng. In: *Journal of turbomachinery* 142.7 (2020). ISSN: 0889-504X (cit. on p. 12).

[35] José Ramón Serrano, Roberto Navarro, Luis Miguel García-Cuevas, and Lukas Benjamin Inhestern. «Contribution to tip leakage loss modeling in radial turbines based on 3D flow analysis and 1D characterization». eng. In: *The International journal of heat and fluid flow* 78 (2019), p. 108423. ISSN: 0142-727X (cit. on p. 12).

[36] Zbigniew Schabowski and Howard Hodson. «The Reduction of Over Tip Leakage Loss in Unshrouded Axial Turbines Using Winglets and Squealers». eng. In: *Journal of turbomachinery* 136.4 (2014). ISSN: 0889-504X (cit. on p. 12).

[37] C. H. Sieverding. «Recent Progress in the Understanding of Basic Aspects of Secondary Flows in Turbine Blade Passages». In: *Journal of Engineering for Gas Turbines and Power* 107.2 (Apr. 1985), pp. 248–257. ISSN: 0742-4795. DOI: 10.1115/1.3239704. eprint: https://asmedigitalcollection.asme.org/gasturbinespower/article-pdf/107/2/248/5702799/248_1.pdf. URL: https://doi.org/10.1115/1.3239704 (cit. on p. 13).

[38] L.S LANGSTON. «Secondary Flows in Axial Turbines-A Review». eng. In: *Annals of the New York Academy of Sciences* 934.1 (2001), pp. 11–26. ISSN: 0077-8923 (cit. on p. 13).

[39] Lin Meng, XiaoDong Zhang, Gong Yan, and Cancan Peng. «Investigation of improving the hydraulic turbine cascade performance using non-axisymmetric endwall contouring». eng. In: *Advances in mechanical engineering* 12.4 (2020), p. 168781402091541. ISSN: 1687-8140 (cit. on pp. 13, 47).

[40] Zhi Tao, Zhendong Guo, Boyang Yu, Liming Song, and Jun Li. «Aero-thermal optimization of a gas turbine blade endwall with non-axisymmetric contouring and purge flow». eng. In: *International journal of heat and mass transfer* 178 (2021), p. 121626. ISSN: 0017-9310 (cit. on pp. 13, 47).

[41] Zhi Tao, Boyang Yu, Yixing Li, Liming Song, and Jun Li. «Effects of non-axisymmetric endwall contouring on aerothermal performance of a gas turbine blade endwall with a purge flow». eng. In: *International journal of thermal sciences* 164 (2021), p. 106921. ISSN: 1290-0729 (cit. on pp. 13, 47).

[42] Jinjin Li, Xin Yan, and Kun He. «Effect of Non-Axisymmetric Endwall Profiling on Heat Transfer and Film Cooling Effectiveness of a Transonic Rotor Blade». eng. In: *Journal of turbomachinery* 142.5 (2020). ISSN: 0889-504X (cit. on pp. 13, 47).

[43] Jiyuan Tu, Guan-Heng Yeoh, and Chaoqun Liu. «Chapter 1 - Introduction». eng. In: *Computational Fluid Dynamics*. Third Edition. Elsevier Ltd, 2018, pp. 1–31. ISBN: 0081012446 (cit. on p. 14).

[44] Rodriguez. *Applied Computational Fluid Dynamics and Turbulence Modeling*. eng. Springer International Publishing, 2019. ISBN: 3-030-28690-8 (cit. on p. 14).

[45] Nasuti F. *Dispense del Corso diPropulsione Aerospaziale*. eng. 2016 (cit. on p. 15).

[46] David Ting. *Basics of Engineering Turbulence*. eng. San Diego: Elsevier Science Technology, 2016. ISBN: 9780128039700 (cit. on p. 15).

[47] Paule Petrie-Repar. *Lecture notes of the course Introduction to Computational Fluid Dynamics and Mathematics*. eng. 2021 (cit. on p. 15).

[48] Kemal Hanjalic and Brian Launder. *Modelling Turbulence in Engineering and the Environment, by Kemal Hanjalic and Brian Launder, Cambridge University Press 2011, ISBN 978-0-521-84575-5.* Jan. 2011. ISBN: 978-0521-84575-5 (cit. on p. 15).

[49] IdealSimulation. *Turbulence Models In CFD.* eng. 2021 (cit. on p. 15).

[50] Jiyuan Tu, Guan-Heng Yeoh, and Chaoqun Liu. «Chapter 3 - Governing Equations for CFD: Fundamentals». eng. In: *Computational Fluid Dynamics.* Third Edition. Elsevier Ltd, 2018, pp. 65–124. ISBN: 0081012446 (cit. on p. 15).

[51] Jiyuan Tu, Guan-Heng Yeoh, and Chaoqun Liu. «Appendix A - Full Derivation of Conservation Equations». eng. In: *Computational Fluid Dynamics.* Third Edition. Elsevier Ltd, 2018, pp. 419–425. ISBN: 0081012446 (cit. on p. 15).

[52] Jiyuan Tu, Guan-Heng Yeoh, and Chaoqun Liu. «Chapter 5 - CFD Techniques: The Basics». eng. In: *Computational Fluid Dynamics.* Third Edition. Elsevier Ltd, 2018, pp. 155–210. ISBN: 0081012446 (cit. on p. 15).

[53] Jiyuan Tu, Guan-Heng Yeoh, and Chaoqun Liu. «Chapter 4 - CFD Mesh Generation: A Practical Guideline». eng. In: *Computational Fluid Dynamics.* Third Edition. Elsevier Ltd, 2018, pp. 125–154. ISBN: 0081012446 (cit. on p. 15).

[54] Liu Chaoqun, Yeoh Guan-Heng, and Tu Jiyuan. «CFD Techniques: The Basics». eng. In: *Computational Fluid Dynamics - A Practical Approach.* 3rd Edition. Elsevier, 2018, pp. 1–1. ISBN: 9780081011270 (cit. on p. 15).

[55] P.R Spalart. «Strategies for turbulence modelling and simulations». eng. In: *The International journal of heat and fluid flow* 21.3 (2000), pp. 252–263. ISSN: 0142-727X (cit. on p. 16).

[56] Mauricio Gutiérrez Salas. *Lecture notes of the course Theory and Practice of Computational Methods in Energy Technology (KTH).* eng. 2021 (cit. on p. 16).

[57] P.R Spalart. «Strategies for turbulence modelling and simulations». eng. In: 21.3 (2000), pp. 252–263. ISSN: 0142-727X (cit. on p. 17).

[58] Jiyuan Tu, Guan Heng Yeoh, and Chaoqun Liu. «CFD Solution Procedure—A Beginning». In: (2013) (cit. on p. 18).

[59] Simscale. *Theory for CFD simulations https://www.simscale.com/.* eng. 2021 (cit. on p. 20).

[60] A. Abou El-Azm Aly, Ahmed Hassan, and Haïscam Abdallah. «Numerical Study of the Semi-Open Centrifugal Pump Impeller Side Clearance». In: May 2015. DOI: 10.13140/RG.2.1.3541.5928 (cit. on p. 21).

[61] Tiziano Ghisu. *Introduction to Meshing.* eng. 2021 (cit. on p. 22).

[62] Wujun Wang. *Lecture notes of the course Theory and Practice of Computational Methods in Energy Technology (KTH).* eng. 2021 (cit. on p. 22).

Appendix A

Experimental measurements

A.1   Additional formulas

In the calculation of the efficiency and of the dimensionless parameters of the flow it was shown which are the main formulas. However, some variables depend on quantities that have not been fully defined. For example, the inlet velocity of the flow is considered axial and its value is not measured directly but is derived from the continuity equation of fluids. For this reason it is necessary to know the **mass flow** rate, which is measured with differential instruments and whose value is calculated with the formulas below. For the calculation of the isentropic **enthalpy** drop, it is needed to know the **temperature and pressure** values in some sections. This is also explained in this additional formulas sections.

A.1.1   Mass flow

Mass flow is calculated according to ISO 5167-1 (1991) and the supplement ISO 5167-1: Amd.1 (1998). The calculation is iterative because the mass flow value depends on the Reynolds number and the Reynolds number is a funcion of the mass flow. The calculation process is described below.

1) Assume a Reynolds number (ex. Rein = 1000000)

2) Set Re = Rein

3) Calculate a C-value (Eq.A.12) with Re.

4) Calculate the mass flow (Eq.A.1 using Eq.A.2 to Eq.A.11)

5) Calculate new Rein with Eq.A.13 (using Eq.A.14) and the calculated mass flow above

Repeat steps 2 to 5 until (| Rein-Re | / Rein) <0.001 when the iteration is stopped and the mass flow is given as output (MF1 or MF2).

Input data

Input data according to the following table is required.

Input (device)	variable	MF1	MF2
Absolut pressure (Pa)	p	TL4101-PMF1	TL4101-PMF2
Differential pressure (Pa)	Δp	TL4101-DPMF1	TL4101-DPMF2
Temperature (°C)	t	TL4101-GT401	TL4101-GT402
Relative humidity (%)	ϕ	TL4101-GH401	TL4101-GH402
Inside pipe diameter (m)	D	0.3017	0.0720
Hole diameter (m)	d	0.1500	0.0357

Table A.1: Input data to calculate mass flow

Simplifications

- Temperature expansion (approx. 16.8 * 10-6 m / ° C) whose impact is judged to be small in the application is disregarded, partly due to moderate temperatures and partly due to the fact that a diameter ratio (d / D) is used in the calculations.

- The medium (air) is assumed to be an ideal gas.

Equations

The mass flow, (kg/s) is calculated according to Eq.A.1:

$$\dot{m} = \frac{C\epsilon\pi d^2}{4\sqrt{1-\beta^4}}\sqrt{2\Delta p\rho} \tag{A.1}$$

where β is the diameter ratio according to Eq.A.2:

$$\beta = \frac{d}{D} \tag{A.2}$$

ϵ is defined (after ISO) as Eq.A.3:

$$\varepsilon = 1 - \left(0.41 - 0.35\beta^4\right)\frac{\Delta p}{\gamma \cdot p} \tag{A.3}$$

where γ is the isentropic exponent that can be defined according to Eq.A.4 for an ideal gas:

$$\gamma = \frac{c_p}{c_p - R} \tag{A.4}$$

and where R (J / kgK) is the gas constant calculated according to Eq. A.5:

$$R = \frac{8314.4}{(1+X)} \cdot \left(\frac{1}{28.97} + \frac{X}{18.016} \right) \tag{A.5}$$

X(kg H2O per kg dry air, TL) is the absolute water content and is calculated as Eq.A.6, via Eq.A.7.

$$X = \frac{18.016}{28.97} \cdot \left(\frac{p_{H_2O}}{\frac{p}{100000} - p_{H_2O}} \right) \tag{A.6}$$

$$p_{H_2O} = \frac{\phi \cdot e^{\left(12.03 - \frac{4025}{t+235} \right)}}{100} \tag{A.7}$$

cp(J / kgK) and Eq.A.4 is calculated according to Eq.A.8 via polynomial in Eq. A.9 & Eq.A.10 [NOTE polynomial is not ISO, only applies in this application].

$$c_p = \frac{(c_{p,TL} + X c_{p,H_2O})}{(1+X)} \tag{A.8}$$

$$c_{p,TL} = 1005.5 + 0.000135 \left(t + 30 \right)^2 \tag{A.9}$$

$$c_{p,H_2O} = 1858.4 + 9.404 \left(\frac{t}{100} \right) + 3.73 \left(\frac{t}{100} \right)^2 \tag{A.10}$$

The density, $\rho(kg/m^3)$, to be used and Eq. A.1 is calculated via the ideal gas law according to Eq. A.11:

$$\rho = \frac{p}{R \cdot (t + 273.15)} \tag{A.11}$$

Then it remains to define the C-value used in Eq. A.1 where otherwise π can be set to 3.1415926535. The C-value is calculated according to ISO as Eq. A.12.

$$C = 0.5961 + 0.0261\beta^2 - 0.216\beta^8 + 0.000521 \cdot F$$
$$F = \left(\frac{10^6 \beta}{\text{Re}} ()^{0.7} \left(0.0188 + 0.0063 \left(\frac{19000\beta}{\text{Re}} ()^{0.8} \right) ()^{3.5} \left(\frac{10^6}{\text{Re}} ()^{0.3} \right) \right) \right) \tag{A.12}$$

β is according to Eq.A.2 and Reynolds number (Re) is calculated according to Eq.A.13 where the dynamic viscosity, μ (kg/ms) is calculated according to the polynomial in Eq.A.14 [NOTE polynomial is not ISO, only applies in this application].

$$\text{Re} = \frac{4\dot{m}}{\pi \mu D} \tag{A.13}$$

$$\mu = 0.00001748 + 0.0000000431 \cdot t \tag{A.14}$$

A.1.2 Isentropic enthalpy drop

To calculate the isentropic enthalpy drop of the turbine, it is necessary to know the average values on the inlet and outlet section of the temperature (1,8) and pressure (4, 7). Also for the degree of reaction it is necessary to know the pressure at the inlet of the stator (4), at the inlet of the rotor (5) and at the outlet of the rotor (7). In this particular case 8 values were measured for each section.

Pressure and temperature averaging

The **pressure** is measured with a set of PSI 9010 modules within the appropriate range. They are re-zero before and after the measurement to check for drift. When not other reference pressure is needed, it is possible to use atmospheric pressure as a reference and this is the measurement continuously. The total **temperature** is measured at two radial positions with K-type thermocouples [19].

Each data point is **time** averaged from 60 sequentially collected samples, with frequency at approximately 1 Hz. In addition, there is a **space** mean temperature and pressure. The layers extracted 8 temperature values for each section (1 and 8) evaluated on circumferences with different radii. On the other hand, also the static pressure is the average of 8 pressure taps, 4 located at the hub, 4 at the sleeve, distributed along the circumference, evaluated for section 4, 5 and 7.
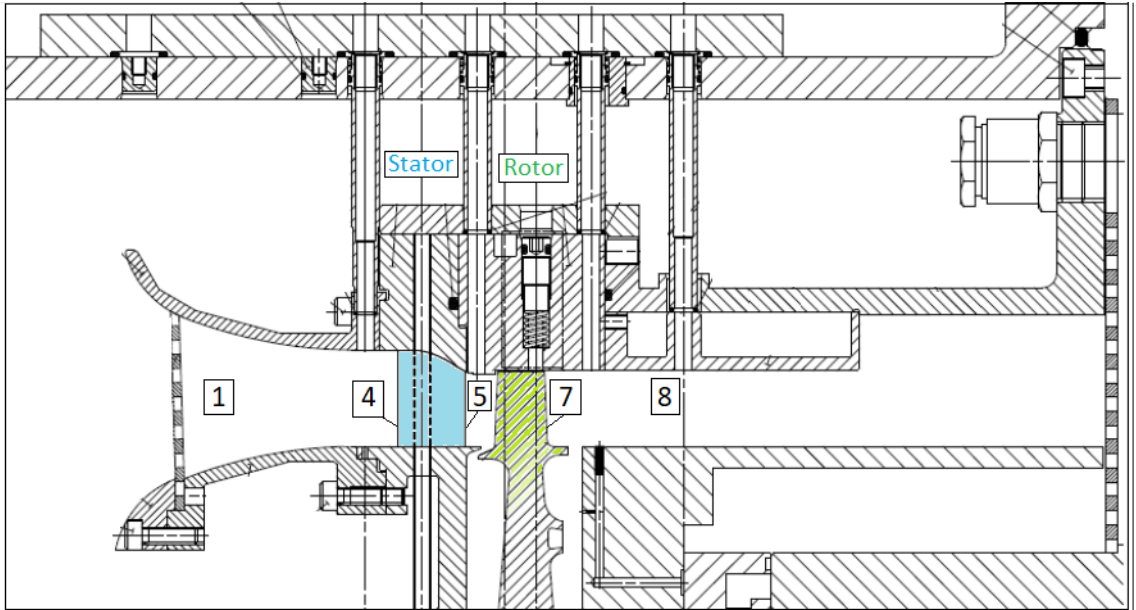

Figure A.1: Sections for pressure and temperature averaging

Appendix B

Simulations setup

B.1 Mesh 1: AutoGrid

B.1.1 From TurboGrid to AutoGrid

The simplest way to create a mesh for later use in ANSYS-CFX is to use the in built package called TurboGrid. This allows, for simple geometries to create meshes quickly and quite well. Unfortunately for this complex geometry, the software does not give good results because in the non-axisymmetric hub area the solution is unsatisfactory.

For the reasons described above, the approach was changed using a new software called Numeca-AutoGrid5. In general, its operation is quite efficient, obtaining good results in a short time. This was not the case with this turbine either due to errors in the CAD file, or to the intrinsic complexity of the geometry.

B.1.2 Errors in AutoGrid

Error 1

"*Error in the selection of surfaces:* the current CAD file of the turbine geometry was not read correctly in the AutoGrid, preventing the selection of some surfaces. It was therefore replaced with another type of file."

Error 2

"*Error for no intersection between hub and leading edge*: caused by a small gap between the blade and the hub for tolerance reasons, it gave an intersection error between hub line and leading edge line. For this reason, the blade was lengthened with a CAD software until it passed the hub line in order to ensure the intersection with the leading edge. "
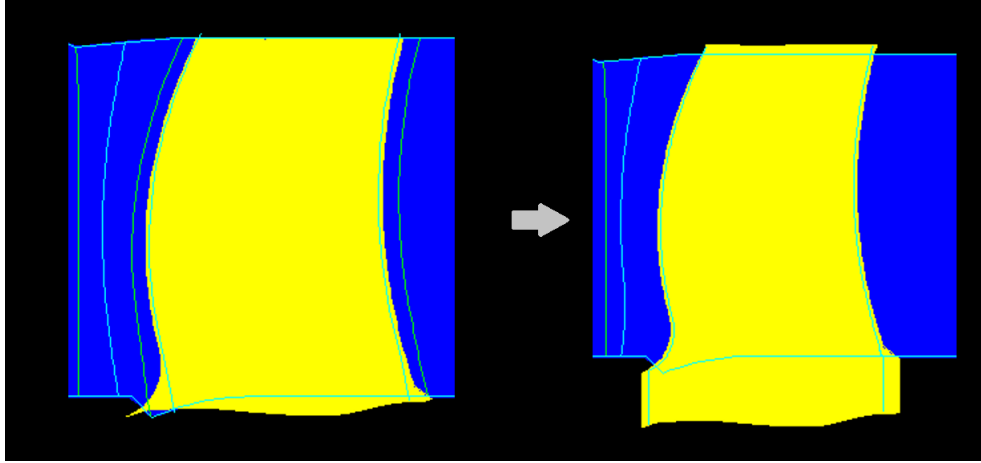

Figure B.1: AutoGrid: Surface elongation

Error 3

"*Meridian line generation error*: for the non-axysimmetric hub it was difficult to create the meridian line because it was formed by numerous surfaces each with its own meridian line. For this reason, first of all a larger surface was created made from the union of all the surfaces. But even in this case the meridian line created automatically in AutoGrid was wrong, so it was defined manually in CAD and then imported separately."
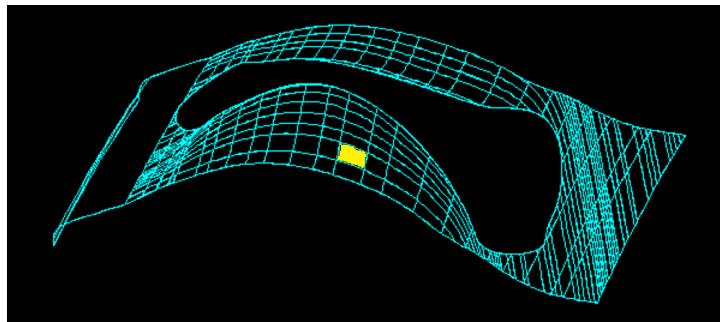

Figure B.2: AutoGrid: Non-axisymmetric hub and sub-surfaces

63

Error 4

"*Error due to discontinuity in the leading edge and trailing edge line:* by associating the edges between the suction side and pressure side of the blade with the leading and trailing edge, AutoGrid detected an error in the definition of these elements. This bug was solved by creating these lines in CAD and importing and associating them in AutoGrid as part of the turbine. "
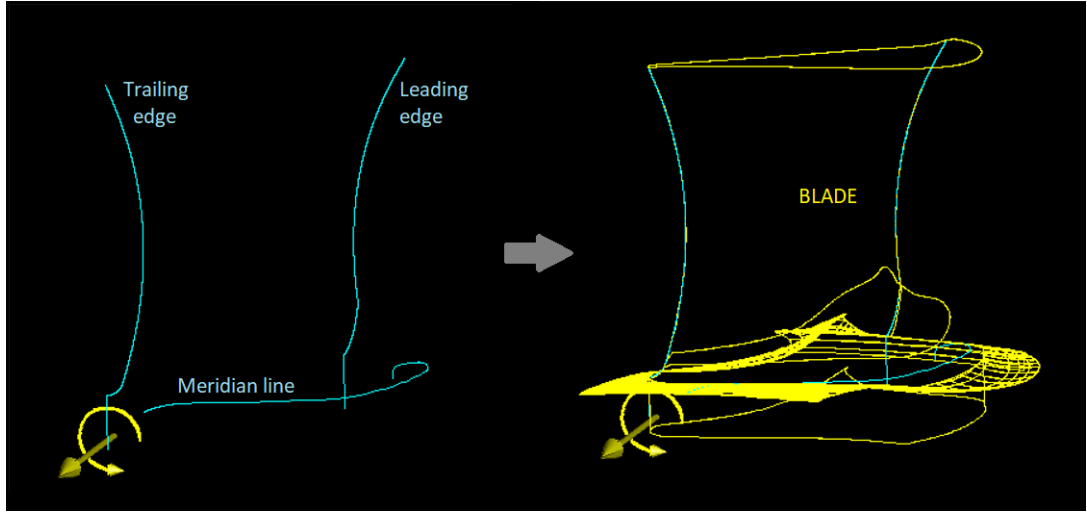

Figure B.3: AutoGrid - Lines definition: meridian, leading edge, trailing edge

Error 5

"*Blade surface association error:* AutoGrid detected errors that are not entirely clear regarding the definition of the blade surface. Working again on the geometry file again in CAD, it was observed that there were multiple overlapping surfaces, leading to association errors in AutoGrid. "

Error 6

"*Error in recognizing the interface between non-axisymmetric hub and blade.*"

Solution 1

"Create a smoother blade-hub interface line higher up to have a smoother surface angle change between blade and hub. This solution did not lead to solving the problem. "
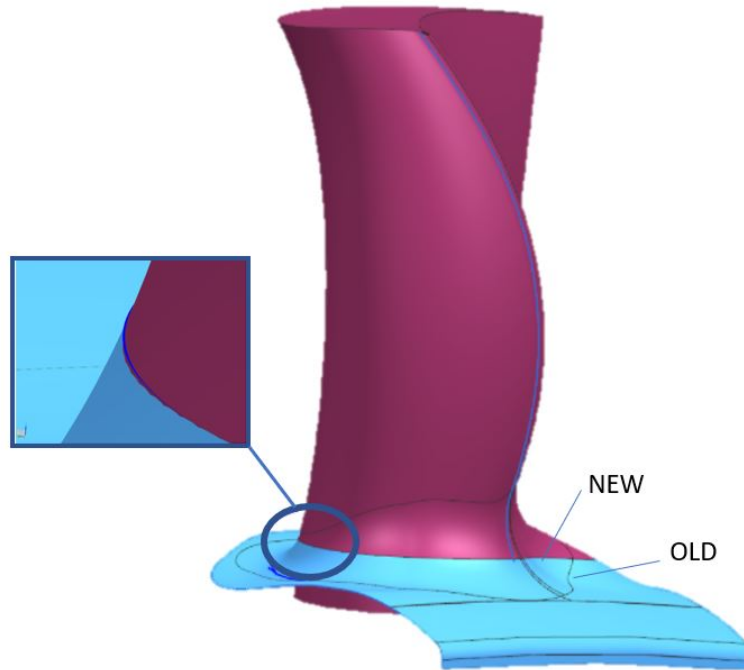

Figure B.4: New interface between blade and hub

Solution 2

"Divide the domain into three zones: stator, upper rotor, lower rotor containing also the non-axisymmetric hub. For the stator and the top of the rotor a mesh was generated in AutoGrid without any problems. For the lower part of the rotor, problematic in AutoGrid, the mesh will be generated with the ICEM program, a process that requires a significant amount of time and specialized personnel."
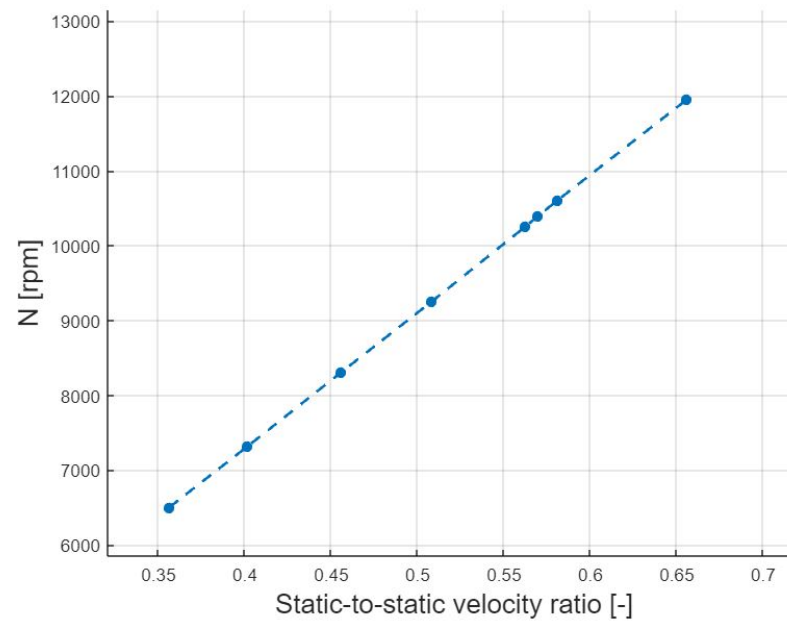
Appendix C

Additional results

C.1 Blisk 6 (2021)

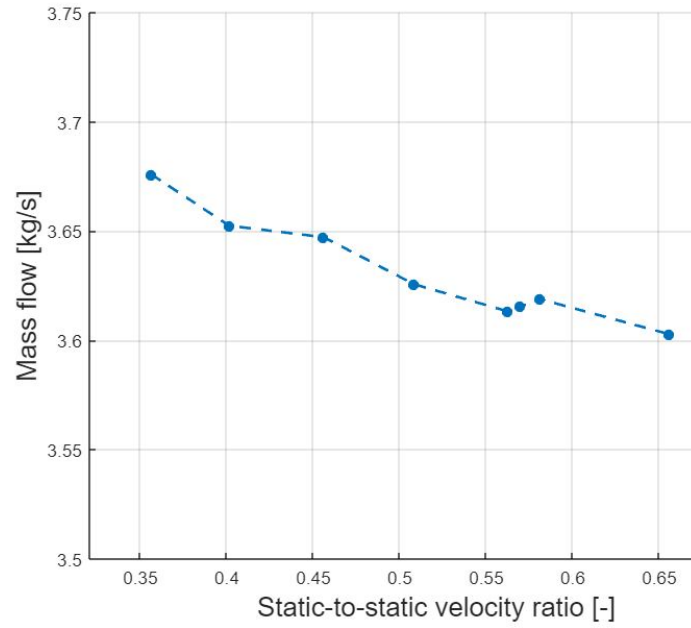**Figure C.1:** Experiments Blisk 6 (2021): Rotation speed

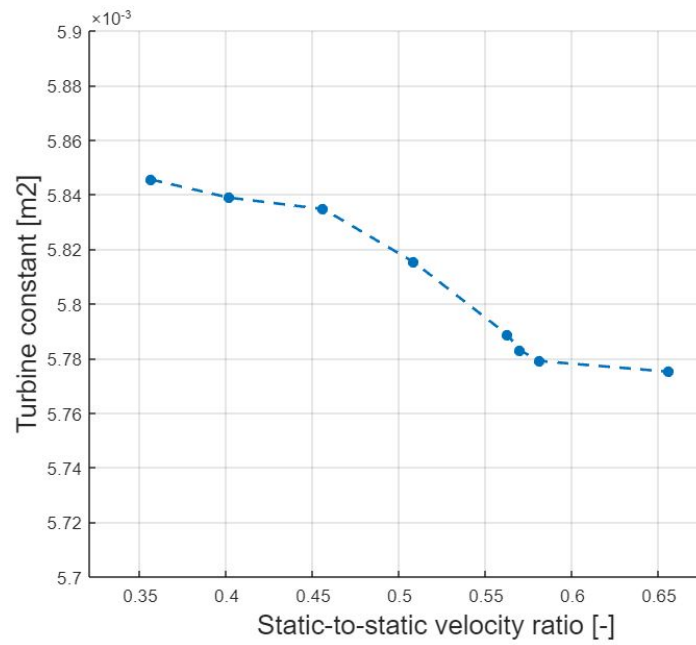**Figure C.2:** Experiments Blisk 6 (2021): Mass Flow

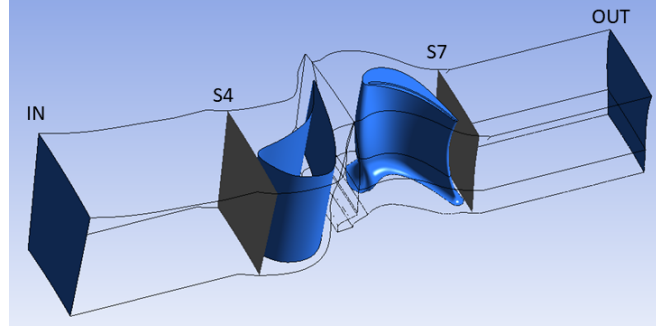**Figure C.3:** Experiments Blisk 6 (2021): Turbine Constant

C.2 Simulations

Figure C.4: Sections simulation: inlet, S4, S7, outlet

	Ptin_sim	Pt4_Sim	Pt4_exp
6500	220448	220394	220445.5
7300	220567	220550	220567.7
8300	220126	220076	220124.1
9250	220605	220481	220602.1
10250	220235	220213	220234.4
10400	220181	220141	220180
10600	220183	220158	220181.5
12500	220505	220475	220503.9

Table C.1: Total pressure: Experiments and Simulation

	Ps4_exp	Ps4_sim	Ps7_sim	Ps7_exp
6500	218774	218871	103158	103195.1
7300	218897.5	219014	102752	103089.1
8300	218458.2	218549	103189	103104.7
9250	218944.1	218598	103626	103183.2
10250	218589.6	218700	104226	103139.4
10400	218539	218630	104351	103125.1
10600	218546.7	218645	104345	103165.9
12500	218870.1	218965	104415	103215.5

Table C.2: Static pressure: Experiments and Simulation